JHEP

Published for SISSA by Springer

Received: January 3, 2017
Revised: January 28, 2017
Accepted: February 15, 2017
Published: March 17, 2017

The N2HDM under theoretical and experimental scrutiny

Margarete Mühlleitner,[a] **Marco O.P. Sampaio,**[b] **Rui Santos**[c,d] **and Jonas Wittbrodt**[a,e]

[a] *Institute for Theoretical Physics, Karlsruhe Institute of Technology, 76128 Karlsruhe, Germany*
[b] *Departamento de Física, Universidade de Aveiro and CIDMA, Campus de Santiago, 3810-183 Aveiro, Portugal*
[c] *ISEL — Instituto Superior de Engenharia de Lisboa, Instituto Politécnico de Lisboa, 1959-007 Lisboa, Portugal*
[d] *Centro de Física Teórica e Computacional, Faculdade de Ciências, Universidade de Lisboa, Campo Grande, Edifício C8, 1749-016 Lisboa, Portugal*
[e] *Deutsches Elektronen-Synchrotron DESY, Notkestraße 85, D-22607 Hamburg, Germany*

E-mail: margarete.muehlleitner@kit.edu, msampaio@ua.pt, rasantos@fc.ul.pt, jonas.wittbrodt@desy.de

Abstract: The N2HDM is based on the CP-conserving 2HDM extended by a real scalar singlet field. Its enlarged parameter space and its fewer symmetry conditions as compared to supersymmetric models allow for an interesting phenomenology compatible with current experimental constraints, while adding to the 2HDM sector the possibility of Higgs-to-Higgs decays with three different Higgs bosons. In this paper the N2HDM is subjected to detailed scrutiny. Regarding the theoretical constraints we implement tests of tree-level perturbativity and vacuum stability. Moreover, we present, for the first time, a thorough analysis of the global minimum of the N2HDM. The model and the theoretical constraints have been implemented in `ScannerS`, and we provide `N2HDECAY`, a code based on `HDECAY`, for the computation of the N2HDM branching ratios and total widths including the state-of-the-art higher order QCD corrections and off-shell decays. We then perform an extensive parameter scan in the N2HDM parameter space, with all theoretical and experimental constraints applied, and analyse its allowed regions. We find that large singlet admixtures are still compatible with the Higgs data and investigate which observables will allow to restrict the singlet nature most effectively in the next runs of the LHC. Similarly to the 2HDM, the N2HDM exhibits a wrong-sign parameter regime, which will be constrained by future Higgs precision measurements.

Keywords: Beyond Standard Model, Higgs Physics

ArXiv ePrint: 1612.01309

doi:10.1007/JHEP03(2017)094

JHEP03(2017)094

Contents

JHEP03(2017)094

1 Introduction

The discovery of the Higgs boson by the LHC experiments ATLAS [1] and CMS [2] not only marked a milestone for elementary particle physics but also opened the possiblity to search for new physics (NP) in the Higgs sector itself. Since, so far, a direct discovery of NP in the form of new particles is missing, the Higgs sector plays an increasingly important role. The manifestations of NP in the Higgs sector can be manifold [3]. An immediate direct signal of NP acting in the Higgs sector would be the discovery of additional Higgs bosons, which can be lighter or heavier than the currently known one that has a mass of 125.09 GeV [4]. Indirect signs may appear through modifications in the Higgs couplings to the Standard Model (SM) particles and hence through the observables of the 125 GeV Higgs boson when compared to the SM values. The modifications can be due to strong dynamics behind

electroweak symmetry breaking (EWSB) like in composite Higgs models [5–16]. In the case of weakly coupled models with extended Higgs sectors, the SM-like Higgs boson mixes with the other Higgs bosons thus changing the couplings to the SM particles. Additionally, new non-SM particles, like e.g. the superpartners in supersymmetric extensions, can contribute to the loop-induced couplings to gluons or photons. Furthermore, the different particle content and the modified couplings induce higher order corrections to the Higgs couplings that can be substantially different from the SM case. Finally, the additional Higgs bosons open the possibility of Higgs-to-Higgs decays. These, and possibly invisible decays due to additional lighter Higgs or other particles that are stable, modify the total width and hence the branching ratios of the SM-like Higgs boson.

With the observed Higgs boson behaving very SM-like [17–20] it is clear that any extension of the Higgs sector beyond the SM (BSM) has to provide at least one CP-even Higgs boson with a mass of 125 GeV that reproduces the LHC rates. Additional Higgs bosons predicted by the model have to be compatible with the LHC exclusion bounds. A strong constraint on NP models is given by the ρ parameter. This singles out models with singlet or doublet extended Higgs sectors when some simplicity is required.[1] Doublet extended models are particularly interesting due to their relation to supersymmetry. In particular, the 2-Higgs-doublet model (2HDM) [21–23] has been extensively studied and considered as a possible benchmark model in experimental analyses. The 2HDM features 5 physical Higgs bosons that, in the CP-conserving version of the model, are given by 2 CP-even, 1 CP-odd and 2 charged Higgs bosons. Upon extending the model by a real scalar singlet field with a $\mathbb{Z}_2$ parity symmetry, there is a symmetric phase containing a viable Dark Matter (DM) candidate. This version of the Next-to-Minimal 2HDM (N2HDM) has been subject to numerous investigations, see e.g. [24–37], while in [38] the phenomenology of the N2HDM with non-vanishing vacuum expectation value (VEV) for the singlet field ($\mathbb{Z}_2$ broken phase) has been discussed. In the $\mathbb{Z}_2$ broken phase, after EWSB the N2HDM Higgs sector consists of 3 neutral CP-even scalars, 1 CP-odd and 2 charged Higgs bosons. The Higgs mass eigenstates, which are now superpositions of the singlet and doublet fields, have an interesting phenomenology that is not only governed by the mixing properties of the doublet fields but also by the amount of singlet admixture to the Higgs mass eigenstates. Thus, the couplings to SM particles can be diluted to such an extent that light Higgs bosons are not excluded by Higgs boson searches at LEP, Tevatron and the LHC in the low-mass range. Such light Higgs bosons then allow for Higgs decays of the heavier Higgs bosons into a pair of light Higgs states. Higgs-to-Higgs decays provide alternative production channels for the heavier Higgs bosons and give access to the trilinear Higgs self-couplings. Their measurement is crucial for our understanding of the Higgs mechanism [39–41]. Furthermore, the larger number of parameters, as compared e.g. to the 2HDM, allows for more flexibility in the Higgs sector while being simultaneously in accordance with the experimental and theoretical constraints. This is also the case for the Next-to-Minimal Supersymmetric Model (NMSSM) [42–57] whose Higgs sector is based

[1] Also models with larger SU(2) multiplets or with triplets and a custodial SU(2) global symmetry satisfy the ρ parameter constraint, but entail larger and more complex Higgs sectors.

JHEP03(2017)094

on two doublets and one complex singlet field. Through the SUSY sector the NMSSM encounters even more parameters. The NMSSM Higgs potential, however, is subject to supersymmetric relations. In particular, the Higgs potential parameters of the two Higgs doublets in the NMSSM are given in terms of the gauge boson couplings, so that neither the NMSSM Higgs masses nor the trilinear Higgs self-couplings can become arbitrarily large. The larger Higgs spectrum of the NMSSM, with an additional pseudoscalar Higgs, and the different Higgs self-couplings induce differences in Higgs-to-Higgs decays as compared to the N2HDM. The supersymmetric relations furthermore lead to constraints in the Higgs boson couplings to the SM particles. Therefore, differences in the Higgs rates and also in the coupling patterns, namely in the coupling sum rules, are to be expected. The N2HDM, on the other hand, does not have to respect supersymmetry relations among the masses and couplings. This leads to much more freedom in the choice of parameters of the model and to very different patterns in the couplings of the SM-like Higgs boson. Another class of models that can also provide such extra freedom is given by the scalar singlet framework where one adds hypercharge-zero singlet scalar fields to the SM, i.e. without introducing any extra doublets [58–74]. Though in some of these models [74] one can still obtain a rich phenomenology of Higgs-to-Higgs decays with several Higgs bosons, the coupling structure of the new Higgs bosons to other SM particles is typically controlled by only a global suppression factor (relative to an SM-like Higgs boson). Thus, this provides still less structure than the N2HDM. Finally, being a model with a 2HDM-like sector, the N2HDM also contains a richer spectrum with a charged and a CP-odd Higgs boson that induce different signatures when compared with scalar singlet models. The N2HDM therefore provides an important benchmark model with a very distinct Higgs boson phenomenology as compared to other commonly studied beyond the SM extensions. The potential of various observables to distinguish between all these models requires a detailed comparison, which is beyond the scope of this paper and deferred to future work.

The LHC Higgs data constrain possible deviations induced by NP to be close to the SM case so that only precision measurements allow to reveal BSM signals in the Higgs sector. This calls not only for advanced experimental techniques but also for very precise predictions from the theory side. Thus parameters and observables have to be computed including higher order corrections. Moreover the allowed parameter space of the model has to be evaluated very carefully by checking for consistency with the relevant theoretical and experimental constraints. Only for these parameter regions predictions become meaningful and can be used as guidelines for the experiments. Constraints from the experimental side arise from the Higgs data. The N2HDM has to provide at least one SM-like Higgs boson with a mass of 125 GeV. The additional Higgs bosons must comply with the LHC exclusion limits. Furthermore B-physics and low-energy physics constraints have to be respected as well as the compatibility with the electroweak precision data. Finally, the symmetric N2HDM, which features a Dark Matter (DM) candidate has to comply with the measured value of the relic density.[2] Theoretical constraints that have to be fulfilled

[2]It is also possible to have a $\mathbb{Z}_2$ symmetric scalar singlet model with two CP-even Higgs bosons and a DM candidate [70, 73]. Such a model can be made compatible with DM observables and help to stabilise the SM potential [73]. However, its coupling structure and spectrum are, again, simpler than in the N2HDM.

JHEP03(2017)094

are: that the Higgs potential is bounded from below, that the chosen vacuum is a global minimum and that perturbative unitarity holds. In the N2HDM, the conditions for the first two requirements can be derived from the literature. There exists, however, no analysis so far of all the minima of the N2HDM.

In this work we will determine the allowed parameter space of the N2HDM in the broken phase without applying any approximations on the singlet admixture to the SM-like Higgs boson. Besides taking into account the experimental constraints, we will, in particular, investigate for the first time in great detail the conditions on the N2HDM potential that guarantee tree-level perturbative unitarity, that the vacuum is stable and that the minimum is the global one. We will present the full analysis of the global minimum of the N2HDM potential, which was performed for the first time in [75] where more details can be found. We have implemented the N2HDM in `HDECAY` [76, 77]. This code, called `N2HDECAY`, computes the N2HDM Higgs decay widths and branching ratios including the state-of-the-art higher order QCD corrections and off-shell decays. Furthermore, the model has been included in `ScannerS` [70, 78] along with the theoretical conditions and the available experimental constraints. Then, this allowed us to perform extensive scans in the parameter space of this model taking into account the experimental and theoretical constraints. We will subsequently investigate the features of the surviving parameter space and the implications for LHC phenomenology.

The outline of the paper is as follows. In section 2 we will introduce the N2HDM together with our notation. Section 3 is dedicated to the description of the theoretical constraints that will be applied here for the first time in full scrutiny without any approximations on the N2HDM Higgs potential. Section 4 describes the parameter scan with the applied constraints. Section 5 is dedicated to the phenomenological analysis. Our conclusions are collected in section 6.

2 The N2HDM Higgs sector

The N2HDM is based on the CP-conserving (or real) 2HDM with a softly broken $\mathbb{Z}_2$ symmetry extended by a real singlet field Φ_S. The extension of the 2HDM by a real scalar singlet that does not acquire a VEV provides a viable DM candidate [24–31, 33–35, 37]. In [38] the phenomenology of the N2HDM with non-vanishing VEV for the singlet field has been discussed by applying some approximations. In particular, the possibility of a singlet admixture to the 125 GeV Higgs boson has been neglected. In the following no such assumptions will be imposed on the N2HDM potential. In terms of the two $\mathrm{SU}(2)_L$ Higgs doublets Φ_1 and Φ_2 and the singlet field Φ_S, the N2HDM potential is given by

$$\begin{aligned} V = {} & m_{11}^2|\Phi_1|^2 + m_{22}^2|\Phi_2|^2 - m_{12}^2(\Phi_1^\dagger\Phi_2 + \text{h.c.}) + \frac{\lambda_1}{2}(\Phi_1^\dagger\Phi_1)^2 + \frac{\lambda_2}{2}(\Phi_2^\dagger\Phi_2)^2 \\ & + \lambda_3(\Phi_1^\dagger\Phi_1)(\Phi_2^\dagger\Phi_2) + \lambda_4(\Phi_1^\dagger\Phi_2)(\Phi_2^\dagger\Phi_1) + \frac{\lambda_5}{2}\left[(\Phi_1^\dagger\Phi_2)^2 + \text{h.c.}\right] \\ & + \frac{1}{2}m_S^2\Phi_S^2 + \frac{\lambda_6}{8}\Phi_S^4 + \frac{\lambda_7}{2}(\Phi_1^\dagger\Phi_1)\Phi_S^2 + \frac{\lambda_8}{2}(\Phi_2^\dagger\Phi_2)\Phi_S^2 \,. \end{aligned} \tag{2.1}$$

JHEP03(2017)094

	Φ_1	Φ_2	Φ_S
$\mathbb{Z}_2$ (explicitly broken, softly)	+	−	+
$\mathbb{Z}_2'$ (spontaneously broken)	+	+	−

Table 1. $\mathbb{Z}_2$ and $\mathbb{Z}_2'$ assignments for the scalar fields in the model.

The first two lines describe the 2HDM part of the N2HDM while the last line contains the contribution of the singlet field Φ_S. This potential is obtained by imposing two $\mathbb{Z}_2$ symmetries on the scalar potential. The first one, called $\mathbb{Z}_2$,

$$\Phi_1 \to \Phi_1\,, \qquad \Phi_2 \to -\Phi_2\,, \qquad \Phi_S \to \Phi_S \tag{2.2}$$

is the trivial generalisation of the usual 2HDM $\mathbb{Z}_2$ symmetry to the N2HDM. It is softly broken by the term involving m_{12}^2 and can be extended to the Yukawa sector to guarantee the absence of tree-level Flavour Changing Neutral Currents (FCNC). The second $\mathbb{Z}_2$ symmetry, $\mathbb{Z}_2'$, is

$$\Phi_1 \to \Phi_1\,, \qquad \Phi_2 \to \Phi_2\,, \qquad \Phi_S \to -\Phi_S \tag{2.3}$$

and is not explicitly broken. If Φ_S does not acquire a VEV this $\mathbb{Z}_2'$ symmetry will give rise to a conserved "darkness" quantum number and to the appearance of a dark matter candidate. If Φ_S acquires a VEV this quantum number is no longer conserved and there is mixing among all CP-even neutral particles. This same behaviour is still possible if $m_{12}^2 = 0$, where both the $\mathbb{Z}_2$ and $\mathbb{Z}_2'$ symmetries in the potential are exact but need to be spontaneously broken. We will not consider such model further in this study. The two $\mathbb{Z}_2$ and $\mathbb{Z}_2'$ quantum numbers assigned to the scalars in the model are shown in table 1.

After EWSB the two doublet fields acquire the real VEVs v_1 and v_2 and the singlet field a real VEV v_S. They can be parametrised as

$$\Phi_1 = \begin{pmatrix} \phi_1^+ \\ \frac{1}{\sqrt{2}}(v_1 + \rho_1 + i\eta_1) \end{pmatrix}, \qquad \Phi_2 = \begin{pmatrix} \phi_2^+ \\ \frac{1}{\sqrt{2}}(v_2 + \rho_2 + i\eta_2) \end{pmatrix}, \qquad \Phi_S = v_S + \rho_S\,, \tag{2.4}$$

in terms of the charged complex fields ϕ_i^+ $(i = 1, 2)$ and the real neutral CP-even and CP-odd fields ρ_I $(I = 1, 2, S)$ and η_i, respectively. Requiring the potential to be minimized at the VEV leads to three minimum conditions given by

$$\frac{v_2}{v_1} m_{12}^2 - m_{11}^2 = \frac{1}{2}(v_1^2\lambda_1 + v_2^2\lambda_{345} + v_S^2\lambda_7) \tag{2.5}$$

$$\frac{v_1}{v_2} m_{12}^2 - m_{22}^2 = \frac{1}{2}(v_1^2\lambda_{345} + v_2^2\lambda_2 + v_S^2\lambda_8) \tag{2.6}$$

$$-m_S^2 = \frac{1}{2}(v_1^2\lambda_7 + v_2^2\lambda_8 + v_S^2\lambda_6)\,, \tag{2.7}$$

with

$$\lambda_{345} \equiv \lambda_3 + \lambda_4 + \lambda_5\,. \tag{2.8}$$

Replacing the doublet and singlet fields in the Higgs potential by the parametrisations (2.4) the mass matrices in the gauge basis are obtained from the second derivatives with respect

JHEP03(2017)094

to the fields in the gauge basis. Due to charge and CP conservation the 7×7 mass matrix decomposes into three blocks: the 2×2 matrix for the charged Higgs bosons, the 2×2 matrix for the CP-odd fields and the 3×3 matrix for the CP-even states. Introducing a real singlet field with a VEV, the charged and pseudoscalar sectors of the model remain unchanged with respect to the 2HDM. Consequently, as in the 2HDM, the charged and pseudoscalar mass matrices can be diagonalised by the rotation matrix

$$R_\beta = \begin{pmatrix} c_\beta & s_\beta \\ -s_\beta & c_\beta \end{pmatrix}, \tag{2.9}$$

with t_β defined as

$$t_\beta = \frac{v_2}{v_1} \tag{2.10}$$

and

$$v^2 = v_1^2 + v_2^2 \,. \tag{2.11}$$

We have introduced the SM VEV $v \approx 246\,\text{GeV}$ and the abbreviations $\sin x \equiv s_x$, $\cos x \equiv c_x$ and $\tan x \equiv t_x$. This yields the massless charged and neutral would-be Goldstone bosons $G^\pm$ and G^0, the charged Higgs mass eigenstates $H^\pm$ and the pseudoscalar mass eigenstate A.

Due to the additional real singlet field, the CP-even neutral sector of the N2HDM is changed with respect to the 2HDM. Instead of a 2×2 mass matrix we now have a 3×3 matrix. In the basis (ρ_1, ρ_2, ρ_S) it can be cast into the form

$$M^2_{\text{scalar}} = \begin{pmatrix} \lambda_1 c_\beta^2 v^2 + t_\beta m_{12}^2 & \lambda_{345} c_\beta s_\beta v^2 - m_{12}^2 & \lambda_7 c_\beta v v_S \\ \lambda_{345} c_\beta s_\beta v^2 - m_{12}^2 & \lambda_2 s_\beta^2 v^2 + m_{12}^2 / t_\beta & \lambda_8 s_\beta v v_S \\ \lambda_7 c_\beta v v_S & \lambda_8 s_\beta v v_S & \lambda_6 v_S^2 \end{pmatrix}. \tag{2.12}$$

In eq. (2.12) we have used eqs. (2.5)–(2.7), to trade the mass parameters m_{11}^2, m_{22}^2 and m_S^2 for v, t_β and v_S. The mass matrix can be diagonalised by an orthogonal matrix R which we parametrise as

$$R = \begin{pmatrix} c_{\alpha_1} c_{\alpha_2} & s_{\alpha_1} c_{\alpha_2} & s_{\alpha_2} \\ -(c_{\alpha_1} s_{\alpha_2} s_{\alpha_3} + s_{\alpha_1} c_{\alpha_3}) & c_{\alpha_1} c_{\alpha_3} - s_{\alpha_1} s_{\alpha_2} s_{\alpha_3} & c_{\alpha_2} s_{\alpha_3} \\ -c_{\alpha_1} s_{\alpha_2} c_{\alpha_3} + s_{\alpha_1} s_{\alpha_3} & -(c_{\alpha_1} s_{\alpha_3} + s_{\alpha_1} s_{\alpha_2} c_{\alpha_3}) & c_{\alpha_2} c_{\alpha_3} \end{pmatrix} \tag{2.13}$$

in terms of the mixing angles α_1 to α_3. Without loss of generality the angles can be chosen in the range

$$-\frac{\pi}{2} \leq \alpha_{1,2,3} < \frac{\pi}{2} \,. \tag{2.14}$$

The matrix R rotates the interaction basis (ρ_1, ρ_2, ρ_S) into the physical mass eigenstates H_1, H_2 and H_3,

$$\begin{pmatrix} H_1 \\ H_2 \\ H_3 \end{pmatrix} = R \begin{pmatrix} \rho_1 \\ \rho_2 \\ \rho_S \end{pmatrix} \tag{2.15}$$

and diagonalises the mass matrix M^2_{scalar},

$$R M^2_{\text{scalar}} R^T = \text{diag}(m_{H_1}^2, m_{H_2}^2, m_{H_3}^2) \,. \tag{2.16}$$

JHEP03(2017)094

$c(H_iVV)$	
H_1	$c_{\alpha_2}c_{\beta-\alpha_1}$
H_2	$-c_{\beta-\alpha_1}s_{\alpha_2}s_{\alpha_3}+c_{\alpha_3}s_{\beta-\alpha_1}$
H_3	$-c_{\alpha_3}c_{\beta-\alpha_1}s_{\alpha_2}-s_{\alpha_3}s_{\beta-\alpha_1}$

Table 2. The effective couplings of the neutral CP-even N2HDM Higgs bosons H_i to the massive gauge bosons $V = W, Z$.

We use a convention where the mass eigenstates are ordered by ascending mass as

$$m_{H_1} < m_{H_2} < m_{H_3}\,. \tag{2.17}$$

In total, the N2HDM is described by 12 independent real parameters. We choose as many parameters with physical meaning as possible. We use the minimisation conditions to trade m_{11}^2, m_{22}^2 and m_S^2 for the SM VEV v, t_β and v_S and replace the quartic couplings by the physical masses and the mixing angles. The soft $\mathbb{Z}_2$ breaking parameter m_{12}^2 is kept as an independent parameter. Thus, we use the following set of input parameters

$$\alpha_1\,,\quad \alpha_2\,,\quad \alpha_3\,,\quad t_\beta\,,\quad v\,,\quad v_S\,,\quad m_{H_{1,2,3}}\,,\quad m_A\,,\quad m_{H^\pm}\,,\quad m_{12}^2\,. \tag{2.18}$$

In appendix A.1 we provide expressions for the quartic couplings in terms of these input parameters.

The singlet field ρ_S does not directly couple to the SM particles. Therefore, any change in the tree-level Higgs couplings compared to the 2HDM is due to the mixing of the three neutral fields ρ_I. Any coupling not involving the CP-even neutral Higgs bosons remains unchanged compared to the 2HDM and can be found e.g. in [23]. We now provide the couplings of the N2HDM Higgs bosons H_i relevant for Higgs decays. We introduce the Feynman rules for the Higgs couplings H_i to the massive gauge bosons $V \equiv W, Z$ as

$$i\,g_{\mu\nu}\,c(H_iVV)\,g_{H^{\rm SM}VV}\,, \tag{2.19}$$

where $g_{H^{\rm SM}VV}$ denotes the SM Higgs coupling factor. In terms of the gauge boson masses M_W and M_Z, the $\mathrm{SU}(2)_L$ gauge coupling g and the Weinberg angle θ_W it is given by

$$g_{H^{\rm SM}VV} = \begin{cases} gM_W & \text{for } V = W \\ gM_Z/\cos\theta_W & \text{for } V = Z \end{cases}\,. \tag{2.20}$$

We obtain

$$c(H_iVV) = c_\beta R_{i1} + s_\beta R_{i2} \tag{2.21}$$

for the effective couplings defined by eq. (2.19). Replacing the R_{ij} by their parametrisation in terms of the mixing angles yields the effective couplings in table 2.

In order to avoid tree-level FCNCs we extend the $\mathbb{Z}_2$ symmetry (2.2) to the Yukawa sector. This leads to the same four types of doublet couplings to the fermions as in the 2HDM. We show these types in table 3. Consequently, the CP-even H_i Yukawa couplings

JHEP03(2017)094

	u-type	d-type	leptons	Q	u_R	d_R	L	l_R
type I	Φ_2	Φ_2	Φ_2	+	−	−	+	−
type II	Φ_2	Φ_1	Φ_1	+	−	+	+	−
lepton-specific	Φ_2	Φ_2	Φ_1	+	−	+	+	−
flipped	Φ_2	Φ_1	Φ_2	+	−	−	+	+

Table 3. In the three leftmost columns, the four Yukawa types of the $\mathbb{Z}_2$-symmetric 2HDM are defined by the Higgs doublet that couples to each kind of fermion. The five rightmost columns show the corresponding $\mathbb{Z}_2$ parity assignments for the fermions. Q and L are the quark and lepton doublets, respectively, u_R is the up-type quark singlet, d_R is the down-type quark singlet and l_R is the lepton singlet. Observe that, in addition, all gauge bosons are $\mathbb{Z}_2$-even for all types. The $\mathbb{Z}_2'$ parities are not included in the table because all fields, except for Φ_S, are even.

	u-type	d-type	leptons
type I	$\frac{R_{i2}}{s_\beta}$	$\frac{R_{i2}}{s_\beta}$	$\frac{R_{i2}}{s_\beta}$
type II	$\frac{R_{i2}}{s_\beta}$	$\frac{R_{i1}}{c_\beta}$	$\frac{R_{i1}}{c_\beta}$
lepton-specific	$\frac{R_{i2}}{s_\beta}$	$\frac{R_{i2}}{s_\beta}$	$\frac{R_{i1}}{c_\beta}$
flipped	$\frac{R_{i2}}{s_\beta}$	$\frac{R_{i1}}{c_\beta}$	$\frac{R_{i2}}{s_\beta}$

Table 4. Coupling coefficients $c(H_i ff)$ of the Yukawa couplings of the N2HDM Higgs bosons H_i as defined in eq. (2.22).

take the same form as the Yukawa couplings of the 2HDM. With the N2HDM Yukawa Lagrangian

$$\mathcal{L}_Y = -\sum_{i=1}^{3} \frac{m_f}{v} c(H_i ff)\, \bar{\psi}_f \psi_f H_i \tag{2.22}$$

we obtain the effective coupling factors $c(H_i ff)$ in terms of the mixing matrix elements R_{ij} and the mixing angle β provided in table 4. Replacing the R_{ij} by their parametrisation in terms of the α_i this results in the effective coupling expressions given for type I and II in table 5.

The Feynman rule for the H_i coupling to the pseudoscalar A and the Z boson is given by

$$\lambda_\mu(H_i Z A) = \frac{\sqrt{g^2 + g'^2}}{2} (p_{H_i} - p_A)_\mu \, \tilde{c}(H_i V H)\,, \tag{2.23}$$

where g' denotes the $\mathrm{U}(1)_Y$ gauge coupling and p_A and p_{H_i}, the four-momenta of the pseudoscalar and the H_i, are both taken as incoming. The tilde over the coupling factor indicates that it is not an effective coupling in the sense that it is not normalized to a corresponding SM coupling, since there is no SM counterpart. The corresponding Feynman rule for the H_i coupling to the charged pair $H^\pm$ and $W^\mp$ reads

$$\lambda_\mu(H_i W^\mp H^\pm) = \mp \frac{g}{2} (p_{H_i} - p_{H^\pm})_\mu \, \tilde{c}(H_i V H)\,, \tag{2.24}$$

where $p_{H^\pm}$ denotes the four-momentum of $H^\pm$ and again all momenta are taken as incoming. The coupling factors $\tilde{c}(H_i V H)$ are provided in table 6.

JHEP03(2017)094

Type I

$c(H_i ff)$	u	d	l
H_1	$(c_{\alpha_2} s_{\alpha_1})/s_\beta$	$(c_{\alpha_2} s_{\alpha_1})/s_\beta$	$(c_{\alpha_2} s_{\alpha_1})/s_\beta$
H_2	$(c_{\alpha_1} c_{\alpha_3} - s_{\alpha_1} s_{\alpha_2} s_{\alpha_3})/s_\beta$	$(c_{\alpha_1} c_{\alpha_3} - s_{\alpha_1} s_{\alpha_2} s_{\alpha_3})/s_\beta$	$(c_{\alpha_1} c_{\alpha_3} - s_{\alpha_1} s_{\alpha_2} s_{\alpha_3})/s_\beta$
H_3	$-(c_{\alpha_1} s_{\alpha_3} + c_{\alpha_3} s_{\alpha_1} s_{\alpha_2})/s_\beta$	$-(c_{\alpha_1} s_{\alpha_3} + c_{\alpha_3} s_{\alpha_1} s_{\alpha_2})/s_\beta$	$-(c_{\alpha_1} s_{\alpha_3} + c_{\alpha_3} s_{\alpha_1} s_{\alpha_2})/s_\beta$

Type II

$c(H_i ff)$	u	d	l
H_1	$(c_{\alpha_2} s_{\alpha_1})/s_\beta$	$(c_{\alpha_1} c_{\alpha_2})/c_\beta$	$(c_{\alpha_1} c_{\alpha_2})/c_\beta$
H_2	$(c_{\alpha_1} c_{\alpha_3} - s_{\alpha_1} s_{\alpha_2} s_{\alpha_3})/s_\beta$	$-(c_{\alpha_3} s_{\alpha_1} + c_{\alpha_1} s_{\alpha_2} s_{\alpha_3})/c_\beta$	$-(c_{\alpha_3} s_{\alpha_1} + c_{\alpha_1} s_{\alpha_2} s_{\alpha_3})/c_\beta$
H_3	$-(c_{\alpha_1} s_{\alpha_3} + c_{\alpha_3} s_{\alpha_1} s_{\alpha_2})/s_\beta$	$(s_{\alpha_1} s_{\alpha_3} - c_{\alpha_1} c_{\alpha_3} s_{\alpha_2})/c_\beta$	$(s_{\alpha_1} s_{\alpha_3} - c_{\alpha_1} c_{\alpha_3} s_{\alpha_2})/c_\beta$

Table 5. The effective Yukawa couplings $c(H_i ff)$ of the N2HDM Higgs bosons H_i, as defined in eq. (2.22), in type I and type II.

	$\tilde{c}(H_i VH)$
H_1	$-c_{\alpha_2} s_{\beta-\alpha_1}$
H_2	$s_{\beta-\alpha_1} s_{\alpha_2} s_{\alpha_3} + c_{\alpha_3} c_{\beta-\alpha_1}$
H_3	$c_{\alpha_3} s_{\beta-\alpha_1} s_{\alpha_2} - s_{\alpha_3} c_{\beta-\alpha_1}$

Table 6. The coupling factors $\tilde{c}(H_i VH)$ as defined in the Feynman rules eqs. (2.23) and (2.24) for the H_i couplings to a pair of Higgs and gauge bosons.

The trilinear Higgs self-couplings relevant for the Higgs decays into a pair of lighter Higgs bosons are quite lengthy and deferred to appendix A.2. We have used these Feynman rules to implement the N2HDM in `HDECAY v6.51` [23]. The resulting code `N2HDECAY` calculates all N2HDM Higgs boson decay widths and branching ratios including state-of-the-art higher order QCD corrections and off-shell decays. Electroweak corrections, which in contrast to the QCD corrections cannot be taken over from the SM, have been consistently neglected. The program can be downloaded from the url:

http://itp.kit.edu/~maggie/N2HDECAY/.

In appendix B a short description of the program with a sample input and output file is provided.

We finally note that by letting $\alpha_{2,3} \to 0$ and $\alpha_1 \to \alpha + \pi/2$ the N2HDM approaches the limit of a 2HDM with an added decoupled singlet. In the 2DHM, the mixing angle α diagonalises the 2×2 mass matrix in the CP-even Higgs sector leading to the two CP-even mass eigenstates h and H, respectively. The shift by $\pi/2$ in the limit is necessary to match the usual 2HDM convention. Hence,

$$\text{N2HDM} \;\to\; \text{2HDM} \;\Longleftrightarrow\; \begin{cases} \alpha_1 \to \alpha + \frac{\pi}{2} \\ \alpha_2 \to 0 \\ \alpha_3 \to 0 \end{cases} . \tag{2.25}$$

JHEP03(2017)094

3 Theoretical constraints

In this section we investigate the conditions on the N2HDM imposed by theoretical considerations. These are the requirements for tree-level perturbative unitarity, that the vacuum is stable and that it is the global minimum of the scalar potential. For the first two requirements the corresponding conditions in the N2HDM can be derived from the literature. In the following we will summarize them before presenting the analysis of the stationary points of the N2HDM (cf. also [75]). The model, along with the theoretical conditions, has been implemented in `ScannerS`. This allows us to perform extensive scans in the parameter space of the N2HDM taking into account both the experimental and the theoretical constraints, as will be described in detail in section 4.

3.1 Tree-level perturbative unitarity

Tree-level perturbative unitarity is ensured by requiring that the eigenvalues of the $2 \to 2$ scalar scattering matrix are below an absolute upper value given by 8π [79]. It can be useful to impose a limit smaller than 8π at tree level to safeguard for possible large enhancements of the scalar couplings through higher order corrections. Following the procedure and notation of [79], we have calculated the full $2 \to 2$ scattering matrix of the fields in the gauge basis,

$$H_1^\pm,\ H_2^\pm,\ \rho_1\,,\ \rho_2\,,\ \rho_S\,,\ \eta_1 \text{ and } \eta_2\,. \tag{3.1}$$

The resulting matrix is block diagonal. The block matrices not containing ρ_S have the eigenvalues

$$b_\pm = \frac{1}{2}\Big(\lambda_1 + \lambda_2 \pm \sqrt{(\lambda_1-\lambda_2)^2 + 4\lambda_5^2}\Big) \tag{3.2}$$

$$c_\pm = \frac{1}{2}\Big(\lambda_1 + \lambda_2 \pm \sqrt{(\lambda_1-\lambda_2)^2 + 4\lambda_4^2}\Big) \tag{3.3}$$

$$e_1 = \lambda_3 + 4\lambda_4 - 3\lambda_5 \tag{3.4}$$

$$e_2 = \lambda_3 - \lambda_5 \tag{3.5}$$

$$f_+ = \lambda_3 + 2\lambda_4 + 3\lambda_5 \tag{3.6}$$

$$f_- = \lambda_3 + \lambda_5 \tag{3.7}$$

$$f_1 = \lambda_3 + \lambda_4 \tag{3.8}$$

$$p_1 = \lambda_3 - \lambda_4\,. \tag{3.9}$$

These are the same eigenvalues as found in the 2HDM. The new contributions due to the singlet field yield the eigenvalues

$$s_1 = \lambda_7 \tag{3.10}$$

$$s_2 = \lambda_8 \tag{3.11}$$

and the eigenvalues $a_{1,2,3}$, which are the real roots of the cubic polynomial

$$\begin{aligned} &4(-27\lambda_1\lambda_2\lambda_6 + 12\lambda_3^2\lambda_6 + 12\lambda_3\lambda_4\lambda_6 + 3\lambda_4^2\lambda_6 + 6\lambda_2\lambda_7^2 - 8\lambda_3\lambda_7\lambda_8 - 4\lambda_4\lambda_7\lambda_8 + 6\lambda_1\lambda_8^2) \\ &+ x(36\lambda_1\lambda_2 - 16\lambda_3^2 - 16\lambda_3\lambda_4 - 4\lambda_4^2 + 18\lambda_1\lambda_6 + 18\lambda_2\lambda_6 - 4\lambda_7^2 - 4\lambda_8^2) \\ &+ x^2\big(-6(\lambda_1+\lambda_2+\lambda_6)\big) + x^3. \end{aligned} \tag{3.12}$$

JHEP03(2017)094

Not all of the above eigenvalues are independent. As noted in [79], we have

$$3f_1 = p_1 + e_1 + f_+ \tag{3.13}$$

$$3e_2 = 2p_1 + e_1 \tag{3.14}$$

$$3f_- = 2p_1 + f_+ \,. \tag{3.15}$$

The conditions on f_1, e_2 and f_- can therefore be dropped, as they follow from the conditions on p_1, e_1 and f_+. Since $\lambda_1, \lambda_2 > 0$ is necessary for the potential to be bounded from below (see eqs. (3.25) and (3.26)) we obtain

$$|c_+| > |c_-| \tag{3.16}$$

$$|b_+| > |b_-| \,. \tag{3.17}$$

The resulting conditions for tree-level perturbative unitarity are thus given by

$$|\lambda_3 - \lambda_4| < 8\pi \tag{3.18}$$

$$|\lambda_3 + 2\lambda_4 \pm 3\lambda_5| < 8\pi \tag{3.19}$$

$$\left|\frac{1}{2}\left(\lambda_1 + \lambda_2 + \sqrt{(\lambda_1 - \lambda_2)^2 + 4\lambda_4^2}\right)\right| < 8\pi \tag{3.20}$$

$$\left|\frac{1}{2}\left(\lambda_1 + \lambda_2 + \sqrt{(\lambda_1 - \lambda_2)^2 + 4\lambda_5^2}\right)\right| < 8\pi \tag{3.21}$$

$$a_{1,2,3} < 8\pi \,, \tag{3.22}$$

where $a_{1,2,3}$ are the real roots of eq. (3.12).

3.2 Boundedness from below

We consider the potential to be bounded from below in the strong sense, which means that the potential is required to be strictly positive as the fields approach infinitiy. The corresponding necessary and sufficient conditions have been given in [80] and translated to our notation in [75]. They depend on the discriminant

$$D = \begin{cases} \lambda_4 - \lambda_5 & \text{for } \lambda_4 > \lambda_5 \\ 0 & \text{for } \lambda_4 \leq \lambda_5 \end{cases} . \tag{3.23}$$

The allowed region is given by

$$\Omega_1 \cup \Omega_2 \tag{3.24}$$

with

$$\Omega_1 = \Big\{\lambda_1, \lambda_2, \lambda_6 > 0; \sqrt{\lambda_1\lambda_6} + \lambda_7 > 0; \sqrt{\lambda_2\lambda_6} + \lambda_8 > 0; \\ \sqrt{\lambda_1\lambda_2} + \lambda_3 + D > 0; \lambda_7 + \sqrt{\frac{\lambda_1}{\lambda_2}}\lambda_8 \geq 0\Big\} \tag{3.25}$$

and

$$\Omega_2 = \Big\{\lambda_1, \lambda_2, \lambda_6 > 0; \sqrt{\lambda_2\lambda_6} \geq \lambda_8 > -\sqrt{\lambda_2\lambda_6}; \sqrt{\lambda_1\lambda_6} > -\lambda_7 \geq \sqrt{\frac{\lambda_1}{\lambda_2}}\lambda_8; \\ \sqrt{(\lambda_7^2 - \lambda_1\lambda_6)(\lambda_8^2 - \lambda_2\lambda_6)} > \lambda_7\lambda_8 - (D + \lambda_3)\lambda_6\Big\} \,. \tag{3.26}$$

JHEP03(2017)094

3.3 Global minimum conditions for the N2HDM potential

In general, the minimum needs not be the global minimum, if the tunnelling time for the vacuum to tunnel into the global minimum [81, 82] is larger than the age of universe. As the calculation of the tunnelling time is beyond the scope of this work, we do not discuss such metastable vacua and restrict to the stronger requirement that the vacuum is at the global minimum. While for the 2HDM it has been proven [83] that the existence of a normal minimum of the form eq. (2.4) precludes the existence of a deeper charge- or CP-breaking minimum, this does not generalise to the N2HDM. Counter-examples that underline this statement can be found in the appendix of [75]. For the analysis of the global N2HDM minimum we therefore have to include the possibility of CP- and charge-breaking minima. We consider the most general constant field configuration, where all fields are real,

$$\langle \Phi_1 \rangle = \begin{pmatrix} 0 \\ v_1 \end{pmatrix}, \qquad \langle \Phi_2 \rangle = \begin{pmatrix} v_{\mathrm{cb}} \\ v_2 + i v_{\mathrm{cp}} \end{pmatrix}, \qquad \langle \Phi_S \rangle = v_S \,. \tag{3.27}$$

Here we have already exploited the $\mathrm{SU}(2)_L \times \mathrm{U}(1)_Y$ gauge symmetry to eliminate four degrees of freedom. Any other possible constant field configuration of the N2HDM can be projected onto this one through a gauge transformation. By v_{cb} we denote the charge-breaking and by v_{cp} the CP-breaking constant fields. In the following we will refer to the constant fields as VEVs although this is technically only correct if the configuration describes a minimum of the scalar potential. By expanding the field configuration eq. (3.27) in the potential one observes a set of $\mathbb{Z}_2$ symmetries for the real fields we are using, and we can thus choose, without loss of generality, all VEVs except for v_2 to be positive. We then proceed to find all possible stationary points of the N2HDM. This detailed analysis is presented in appendix C.

We want the minimum to conserve both electric charge and CP and to give rise to three CP-even massive scalars. From the vacuum structure point of view this means that $v_1 \neq 0$, $v_2 \neq 0$ and $v_S \neq 0$ while $v_{\mathrm{cb}} = 0$ and $v_{\mathrm{cp}} = 0$ at the chosen minimum. In order to ensure that this is the global minimum we proceed as follows:

- We choose the model parameters such that there is a minimum with $v_1 \neq 0$, $v_2 \neq 0$, $v_S \neq 0$, $v_{\mathrm{cb}} = 0$, $v_{\mathrm{cp}} = 0$ and $246\,\mathrm{GeV} = v = \sqrt{v_1^2 + v_2^2}$.
- Using the stationarity conditions presented in appendix C we look for all other possible stationary points of the potential with this set of parameters.
- We discard all sets of parameters for which we find a stationary point below the minimum.

This procedure leads to a global minimum that is CP-conserving, preserves electric charge and allows for the singlet to mix with the CP-even scalars from the doublets. We note here that, in the N2HDM, the classification of the possible types of minima, in terms of preservation or breaking of electric charge or CP, follows that of the 2HDM regardless of the value of v_S — see also appendix C.

JHEP03(2017)094

4 The parameter scan

In order to perform phenomenological analyses we need viable parameter points, i.e. points in agreement with theoretical and experimental constraints. To obtain these points we use the program `ScannerS` to perform extensive scans in the N2HDM parameter space and check for compatibility with the constraints. We denote the discovered SM-like Higgs boson with a mass of [4]

$$m_{h_{125}} = 125.09\,\text{GeV} \tag{4.1}$$

by h_{125}. In the following, we exclude all parameter configurations where this Higgs signal is built up by multiple resonances by demanding the mass window $m_{h_{125}} \pm 5\,\text{GeV}$ to be free of any Higgs bosons except for h_{125}. Furthermore, we do not include electroweak corrections in the parameter scans nor in the analysis, as they are not (entirely) available for all observables and cannot be taken over from the SM.

We check for the theoretical constraints on the N2HDM at tree level as described in section 3. Tree-level perturbative unitarity is verified by using eqs. (3.18)–(3.22). This method yields a shorter run-time than the model-independent numeric check implemented in `ScannerS`. We checked that both methods lead to the same results. Equations (3.25) and (3.26) are used to guarantee that the potential is bounded from below. The vacuum state found by `ScannerS` is required to be the global minimum, otherwise it is rejected. As described in 3.3, the check is performed by comparing the value of the scalar potential at the `ScannerS` vacuum with the values at all of the stationary points.

Many of the experimental constraints applied on the 2HDM also hold for the N2HDM. The constraints on R_b [84, 85] and $B \to X_s\gamma$ [85–88] are only sensitive to the charged Higgs boson so that the 2HDM calculation and the resulting 2σ exclusion bounds in the $m_{H^\pm} - t_\beta$ plane can be taken over to the N2HDM. Note that the latest calculation [88] enforces

$$m_{H^\pm} > 480\,\text{GeV} \tag{4.2}$$

in the type II and lepton specific 2HDM. In the type I model on the other hand the bound is much weaker and more strongly dependent on $\tan\beta$. The oblique parameters S, T and U are calculated with the general formulae in [89, 90], and 2σ compatibility with the SM fit [91] including the full correlations is demanded.

The N2HDM must comply with the LHC Higgs data. This requires one scalar state to match the observed signal rates for a Higgs boson of about 125 GeV. Furthermore, the remaining Higgs bosons must be consistent with the exclusion bounds from the collider searches at Tevatron, LEP and LHC, where the strongest constraints arise from the LHC Run 1 data. `ScannerS` provides an interface with `HiggsBounds v4.3.1` [92–94] which we use to check for agreement with all 2σ exclusion limits from LEP, Tevatron and LHC Higgs searches. The required input for `HiggsBounds` are the cross section ratios (relative to a SM Higgs boson of the same mass) of the different production modes, the branching ratios and the total widths for all scalars. We compute the latter two with the program `N2HDECAY`. The production cross sections through gluon fusion (ggF) and b-quark fusion (bbF) are obtained at next-to-next-to-leading order (NNLO) QCD from `SusHi v1.6.0` [95, 96] which

JHEP03(2017)094

is interfaced with ScannerS.[3] The remaining cross section ratios at leading order (and also at higher order in QCD) are given by the effective couplings squared. For example for the production in association with a fermion pair it is $c(H_i f\bar{f})^2$ (table 4), and for the gauge boson mediated cross sections (vector boson fusion and associated production with a vector boson) it is $c(H_i VV)^2$ (eq. (2.21)).

Compatibility of the discovered Higgs signal with h_{125} is checked by using the individual signal strengths fit of ref. [97]. The needed decay widths and branching ratios are taken from N2HDECAY. The fermion initiated cross section normalized to the SM,

$$\mu_F = \frac{\sigma_{\rm N2HDM}(ggF) + \sigma_{\rm N2HDM}(bbF)}{\sigma_{\rm SM}(ggF)}\,, \tag{4.3}$$

is obtained with the NNLO QCD cross sections taken from SusHi. In the normalization we neglect the bbF cross section, which in the SM is very small compared to gluon fusion. The production through vector boson fusion (VBF) or through associated production with a vector boson (VH) normalized to the SM, μ_V, is given by

$$\mu_V = \frac{\sigma_{\rm N2HDM}(VBF)}{\sigma_{\rm SM}(VBF)} = \frac{\sigma_{\rm N2HDM}(VH)}{\sigma_{\rm SM}(VH)} = c^2(H_i VV)\,, \tag{4.4}$$

where H_i is identified with h_{125}. The QCD corrections to massive gauge boson-mediated production cross sections cancel upon normalization to the SM. The properties of the h_{125} are checked against the six fit values of

$$\frac{\mu_F}{\mu_V}\,, \quad \mu_F^{\gamma\gamma}\,, \quad \mu_F^{ZZ}\,, \quad \mu_F^{WW}\,, \quad \mu_F^{\tau\tau}\,, \quad \mu_F^{bb}\,, \tag{4.5}$$

given in [97], with μ_F^{xx} defined as

$$\mu_F^{xx} = \mu_F \frac{\mathrm{BR}_{\rm N2HDM}(H_i \to xx)}{\mathrm{BR}_{\rm SM}(H_i \to xx)}\,. \tag{4.6}$$

For $H_i \equiv h_{125}$ we require agreement with the fit results of [97] at the $2 \times 1\sigma$ level.

In the numerical analysis we will show results for type I and type II N2HDM models. For the scan with the input parameters from eq. (2.18) we fix v to the SM value and choose t_β in the range

$$0.25 \leq t_\beta \leq 35\,. \tag{4.7}$$

As the lower bound on t_β from the R_b measurement is stronger than the lower bound in eq. (4.7), the latter has no influence on the physical parameter points. We transform the mixing matrix generated by ScannerS to the parametrisation of eq. (2.13) such that the mixing angles are allowed to vary in the ranges

$$-\frac{\pi}{2} \leq \alpha_{1,2,3} < \frac{\pi}{2}\,. \tag{4.8}$$

[3] SusHi computes the cross sections for the 2HDM. As the only change of the N2HDM with respect to the 2HDM besides an additional CP-even Higgs boson are the values of the effective couplings to the fermions SusHi can also be used to compute the cross sections for the N2HDM Higgs bosons.

JHEP03(2017)094

We identify one of the neutral Higgs bosons H_i with h_{125} and allow the remaining neutral Higgs bosons to have masses within

$$30\,\text{GeV} \leq m_{H_i \neq h_{125}}\,, \qquad m_A \leq 1\,\text{TeV}. \tag{4.9}$$

In the type II model, the charged Higgs mass is chosen in the range

$$480\,\text{GeV} \leq m_{H^\pm} < 1\,\text{TeV}, \tag{4.10}$$

while we choose

$$80\,\text{GeV} \leq m_{H^\pm} < 1\,\text{TeV} \tag{4.11}$$

in type I. The singlet VEV v_S is generated in the interval

$$1\,\text{GeV} \leq v_S \leq 1.5\,\text{TeV}. \tag{4.12}$$

The value of m_{12}^2 is chosen as

$$0\,\text{GeV}^2 \leq m_{12}^2 < 500000\,\text{GeV}^2. \tag{4.13}$$

The condition $m_{12}^2 > 0$ is found to be necessary for the minimum to be the global minimum of the scalar potential.

5 Phenomenological analysis

We start with the investigation of the parameter distributions and from now on denote the lighter of the two non-h_{125} CP-even Higgs bosons by $H_\downarrow$ and the heavier one by $H_\uparrow$.

The inspection of the mass distributions resulting from our scan for type II shows that the masses can take all values between 30 GeV and 1 TeV. Furthermore, we note that it is possible that both $H_\downarrow$ and $H_\uparrow$ are lighter than h_{125} and also that $H_\downarrow$ and A have masses below 125 GeV. Due to the lower bound $m_{H^\pm} \geq 480\,\text{GeV}$ and the constraints from the EWPT, which force at least one of the non-SM-like neutral Higgs bosons to have mass close to the charged Higgs mass, there is no scenario with all non-SM-like neutral Higgs masses below 125 GeV.

In type I, overall we have lighter Higgs spectra because of the much weaker lower bound on the charged Higgs mass of $m_{H^\pm} \gtrsim 80\,\text{GeV}$. Consequently, here we can also have situations where h_{125} is the heaviest Higgs boson in the spectrum.

5.1 The wrong-sign Yukawa coupling regime

The wrong-sign Yukawa couplings regime, which was discussed in [98–100] for the CP-conserving 2HDM, is the parameter region where the coupling of the h_{125} to the massive gauge bosons is of opposite sign with respect to the coupling to fermions, $c(h_{125} f \bar{f})$. This region is in contrast to the SM case where both couplings have the same sign, which can have interesting phenomenological consequences such as the non-decoupling of heavy particles [98, 101]. This region is not excluded by the experimental data for a type II model with an opposite sign Yukawa coupling to down-type fermions. For the coupling to

JHEP03(2017)094

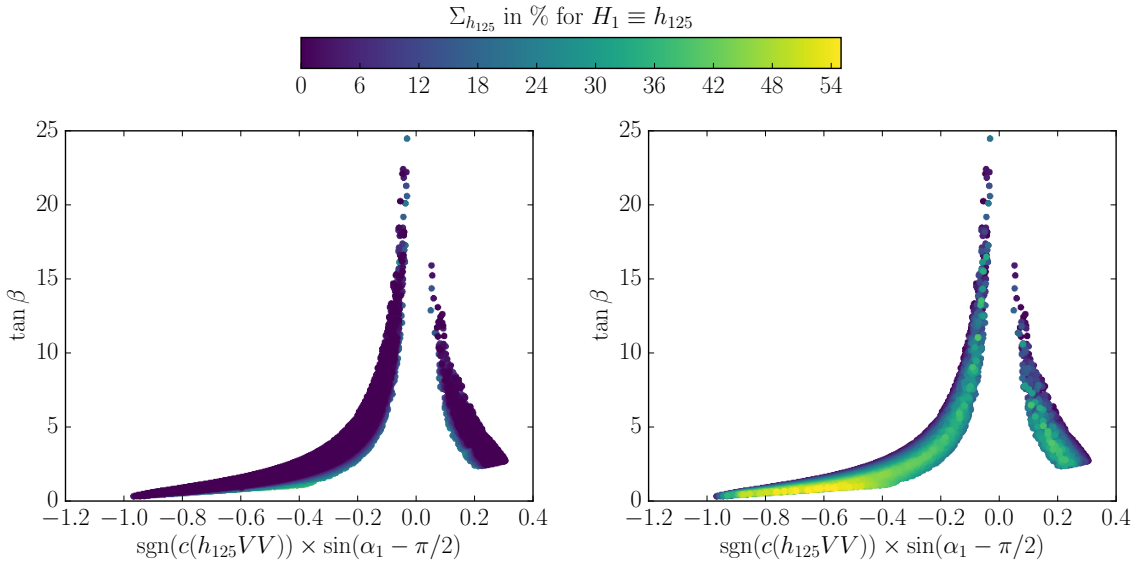

Figure 1. The wrong sign limit in the N2HDM as a function of the singlet admixture. The SM-like Higgs boson is given by $h_{125} \equiv H_1$.

up-type fermions this wrong-sign scenario is only realized for $\tan\beta < 1$ which is excluded. In the type I N2HDM the Yukawa couplings to up- and down-type fermions are the same so that the wrong-sign coupling regime cannot be realized for any of the quark types, as it requires $\tan\beta < 1$. We investigate the extent to which this scenario can be realized in the N2HDM type II. In the 2HDM the wrong-sign regime is obtained for parameter values where $\sin\alpha > 0$, while the correct-sign regime is realized in the opposite case. In order to match the 2HDM description, cf. eq. (2.25), we use the condition

$$\text{sgn}\left(c(h_{125}VV)\right) \cdot \sin\left(\alpha_1 - \frac{\pi}{2}\right) > 0 \tag{5.1}$$

for the wrong-sign limit. Figure 1 displays $\tan\beta$ versus $\text{sgn}\left(c(h_{125}VV)\right) \cdot \sin\left(\alpha_1 - \frac{\pi}{2}\right)$ for all parameter points from our N2HDM type II scan that survive the imposed constraints and where the SM-like Higgs is given by $H_1 = h_{125}$.[4] The colour code quantifies the singlet admixture $\Sigma_{h_{125}}$ of the SM-like Higgs boson h_{125}. We define the singlet admixture $\Sigma_{h_{125}}$ through

$$\Sigma_{h_{125}} \equiv |R_{h_{\text{SM}},3}|^2, \tag{5.2}$$

i.e. the absolute value squared of the mixing matrix element describing the mixing of the singlet field with the SM-like Higgs state. In the right plot we have inverted the colour ordering. In the left panel of figure 1 we observe a large number of points in the 2HDM limit, i.e. with small singlet admixture. Such points are distributed in two branches with a shape that agrees with the 2HDM. This allows to verify the identification of the left branch with the correct-sign regime and of the right branch with the wrong-sign regime.

[4]Quantities which explicitly involve the mixing angles α_i are inherently dependent on the mass ordering. For this reason we only consider the most frequent case $h_{125} = H_1$ in figures 1 and 2.

JHEP03(2017)094

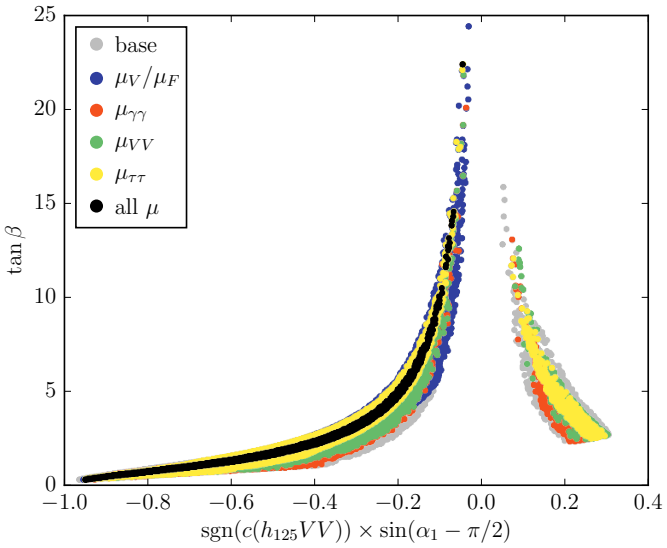

Figure 2. Constraining the N2HDM parameter space with $h_{125} = H_1$; grey: all scan points respecting the experimental and theoretical constraints; remaining colours: additional constraints of $0.95 \leq \mu_V/\mu_F \leq 1.05$ (blue) and $0.95 \leq \mu_{XX} \leq 1.05$ with $X = \gamma$ (orange), $X = V = Z$ (green), $X = \tau$ (yellow) and for all μ_{XX} and μ_V/μ_F (black).

The inverted colour ordering in figure 1 (right) allows us to investigate the repartition of the singlet admixture over the two limiting cases. Overall we see that the singlet admixture can be considerable. In the wrong-sign regime it reaches up to about 30% while in the correct-sign regime it can even be as large as 55%. The points with the largest singlet admixture can be found for small values of $\tan\beta$. In the following analysis we will comment further on the interesting phenomenology of the wrong-sign regime.

Constraining the wrong-sign regime. An important question to ask is to which extent will the collection of more precise data, obtained at the LHC Run II and in the high-luminosity phase, be able to constrain the N2HDM parameter space and in particular the wrong-sign regime. In figure 2 we show again the allowed region in the $\tan\beta$ versus $\mathrm{sgn}\left(c(h_{125}VV)\right) \cdot \sin(\alpha_1 - \pi/2)$ projection of the parameter space, where the grey points respect all theoretical and experimental constraints, in particular the reduced signal strengths from the six-parameter fit of ref. [97] for the SM-like Higgs (here $H_1 \equiv h_{125}$). We then successively constrain the μ-values further, by assuming that future more precise measurements are able to achieve a precision of 5%, with a central value of 1. Hence

$$\begin{aligned} 0.95 \leq \mu_{XX} \leq 1.05 \quad & \text{for } X = \gamma \text{ (orange)}, \; V = Z \text{ (green)}, \; \tau \text{ (yellow)} \\ 0.95 \leq \mu_V/\mu_F \leq 1.05 \quad & \text{(blue)} \\ 0.95 \leq \text{all} \leq 1.05 \quad & \text{(black)} \end{aligned} \tag{5.3}$$

The plot shows that the correct-sign regime given by the left branch is most strongly constrained by the $\tau\tau$ final state. While the wrong-sign limit is also very sensitive to this observable its compatibility with the data is fundamentally different as there are no black

JHEP03(2017)094

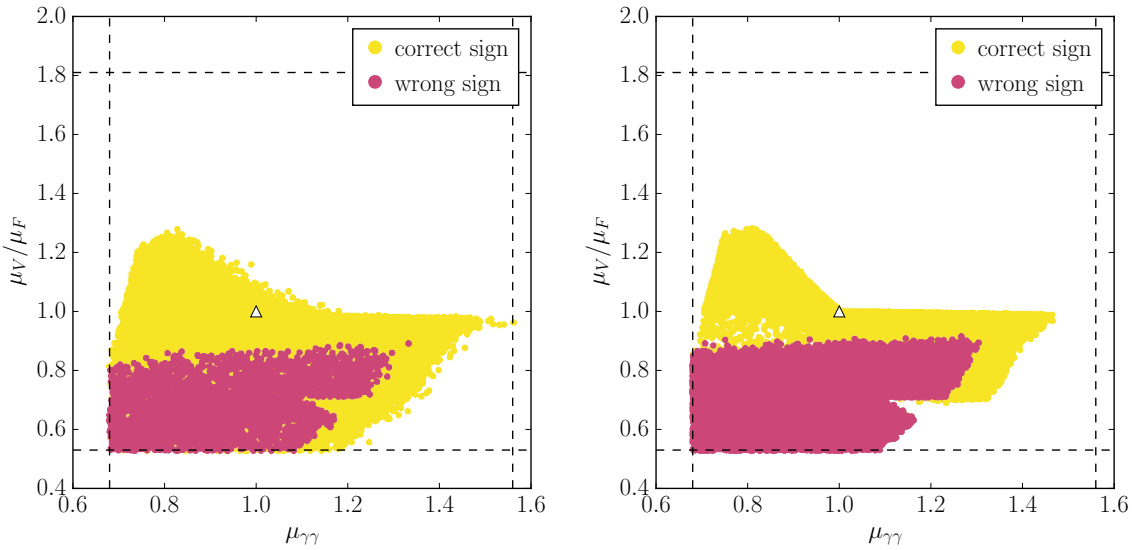

Figure 3. The correct-sign (yellow) and the wrong-sign regime (pink) in the μ_V/μ_F-$\mu_{\gamma\gamma}$ plane for the N2HDM (left) and the 2HDM (right). The h_{125} can be any of the H_i (N2HDM) and $h_{125} \equiv h$ or H (2HDM). The white triangle denotes the SM point. The dashed lines are the current limits on the μ values

nor blue points in the right branch. This behaviour is represented in different form in figure 3, in which we have plotted μ_V/μ_F versus $\mu_{\gamma\gamma}$. The depicted yellow areas show the points from the parameter scan compatible with all constraints in the correct-sign regime, for the N2HDM (left plot) and, for comparison, also for the 2HDM (right).[5] The pink points represent the wrong-sign regime. Here and from now on h_{125} can be any of the CP-even, neutral Higgs bosons (i.e. any H_i in the N2HDM and h or H in the 2HDM). The white triangle denotes the SM result. The yellow and pink regions completely overlap in the N2HDM in contrast to the 2HDM. Here we have less parameters and hence less freedom to reach compatibility with the constraints than in the N2HDM so that the yellow area is more restricted.[6] The allowed area of the wrong-sign regime, on the other hand, is the same in both models. The reason is that in the N2HDM the singlet admixture can at most reduce the Higgs couplings to SM particles and hence the μ-values. As the wrong-sign regime in the 2HDM is already touching the lower bounds in the presented μ-values the N2HDM cannot add anything new to this region. From these figures we immediately infer that in the wrong-sign regime the ratio μ_V/μ_F cannot reach 1, which explains the missing blue and black points in figure 2. The measurement of μ_V/μ_F is hence a powerful observable to constrain the wrong-sign regime with values of $\mu_V/\mu_F \gtrsim 0.9$, excluding this scenario. We note that the pink region in figure 3 is rather insensitive to an increase in the precision of μ_{VV} to 5% around 1.

[5]The constraints applied in the 2HDM are the same as for the N2HDM, as well as the scan ranges (which are identical up to the additional mixing angles and masses in the N2HDM).

[6]The upper two limiting lines of the correct-sign regime in the 2HDM are due to the unitarity of the mixing matrix, whose elements enter the Higgs couplings.

JHEP03(2017)094

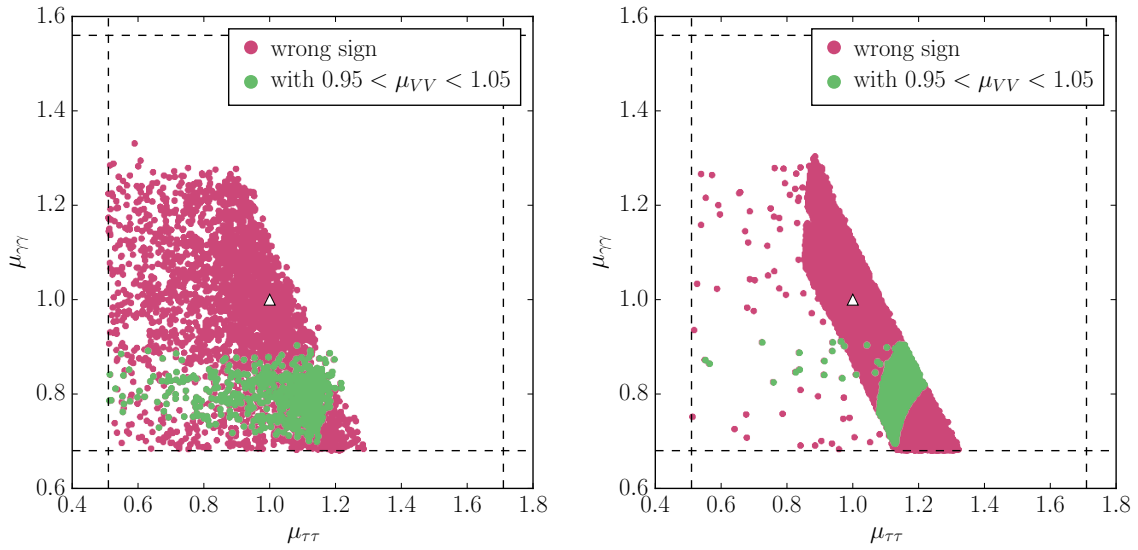

Figure 4. The wrong-sign regime in the $\mu_{\gamma\gamma}$-$\mu_{\tau\tau}$ plane for the N2HDM (left) and the 2HDM (right), where h_{125} can be any of the H_i (N2HDM) and $h_{125} \equiv h$ (2HDM). The green points restrict the allowed area (pink) further by imposing a higher precision in μ_{VV}, $0.95 \leq \mu_{VV} \leq 1.05$. The dashed lines are the current limits on the μ-values.

In figure 4 the pink points show the wrong-sign regime in the $\mu_{\gamma\gamma}$ versus $\mu_{\tau\tau}$ plane. The left panel is for the N2HDM, with h_{125} being any of the H_i, whereas the right panel is for the 2HDM, with[7] $h_{125} \equiv h$. We show on top, in green, a further restriction of the sample assuming that future measurements can constrain the μ_{VV}, $V = Z$, value to 5% around the SM value. Again we observe that the 2HDM area, with a smaller number of parameters, is more constrained than the N2HDM, with the upper bounds in both models being about the same. More importantly, we note that the increase in the precision of μ_{VV} forces the reduced photonic rate to be below about 0.9.[8] Thus, the the wrong-sign regime can be excluded by increasing the precision in the μ_{VV} measurement and observing $\mu_{\gamma\gamma} \gtrsim 0.9$. The outliers in figure 4 are points where h_{125} has a substantial decay width into an (off-shell) pair of light Higgs bosons. The resulting increase of the total width reduces the branching ratio into $\tau\tau$ and thus $\mu_{\tau\tau}$. In the majority of the scenarios the light Higgs boson is the pseudoscalar A. If, however, h_{125} is not the lightest CP-even neutral Higgs boson, decay widths of $h_{125} \to H_1 H_1$ ($h_{125} \to hh$ in the 2HDM) can also be substantial.

5.2 Phenomenology of the h_{125} singlet admixture

Type II N2HDM. The large number of parameters in the N2HDM allows for considerably non-standard properties in the phenomenology of the SM-like Higgs boson. In particular, in type II, which we discuss first, significant singlet admixtures of up to 55% are still compatible with the LHC Higgs data. This can be inferred from figures 5 and 6. Figure 5 displays the correlation between pairs of the effective couplings squared of h_{125}

[7] The plot for $h_{125} \equiv H$ looks similar.

[8] This was already observed for the 2HDM in [98, 99].

JHEP03(2017)094

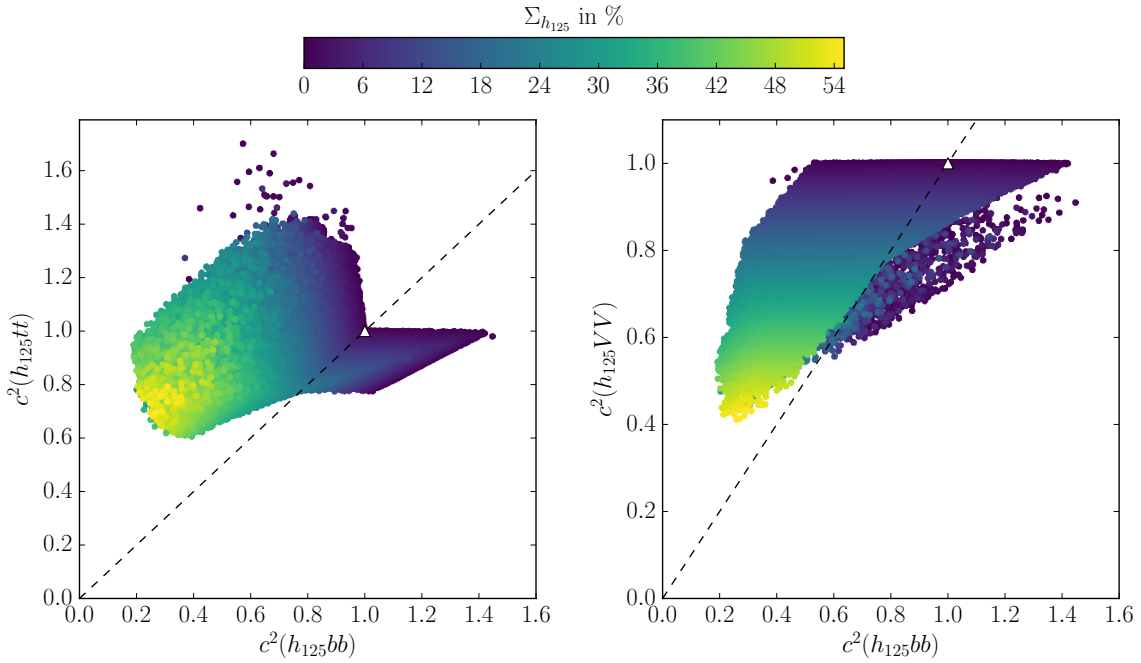

Figure 5. Type II: singlet admixture $\Sigma_{h_{125}}$ as a function of the effective couplings squared. The white triangle denotes the SM value. The dashed line respresents equal scaling of the couplings.

to the SM particles. The left plot shows the coupling to top quarks versus the coupling to bottom quarks, and the right plot shows the coupling to the massive gauge bosons versus the coupling to bottom quarks. We remind that h_{125} can be any of the neutral CP-even Higgs bosons. The influence of the singlet admixture is quantified by the colour code. In figure 6 (left) we show the reduced signal rate in τ final states, $\mu_{\tau\tau}$, versus the one into massive vector bosons, μ_{VV}. In figure 6 (right) we plot the ratio μ_V/μ_F of the vector boson induced production over the fermionic production, each normalized to the SM, versus the photon final state signal strength $\mu_{\gamma\gamma}$. The white triangle indicates the SM values of the signal strengths. The dashed lines are the experimental limits on the respective signal strengths. They show that the N2HDM parameter space is constrained by the upper and lower limits on μ_{VV} and $\mu_{\gamma\gamma}$ and the lower limits on $\mu_{\tau\tau}$ and μ_V/μ_F, respectively. As can be inferred from figure 6 (left) enhanced rates in the τ final state are still allowed by the experimental data where the largest enhancement is reached for small admixture, i.e. in the 2HDM-like regions. The area of the enhanced $\mu_{\tau\tau}$ can be divided in three regions that shall be explained separately. The largest enhancement of up to 40% is obtained for simultaneously enhanced μ_{VV}. The enhancement is due to the production mechanism and corresponds to the enhanced couplings to top quarks in figure 5 (left) while the involved decays remain SM-like. This is confirmed by figure 7 (left), which shows the value of $\mu_{\tau\tau}$ in the plane of the effective couplings squared, $c^2(h_{125}tt)$ and $c^2(h_{h125}bb)$, for parameter points in the correct-sign regime. The largest $\mu_{\tau\tau}$, given by the yellow points, are found for large effective couplings to top quarks. The 2HDM-like region in figure 6, where we have enhanced $\mu_{\tau\tau}$ values but reduced μ_{VV}, is due to enhanced effective couplings to τ

JHEP03(2017)094

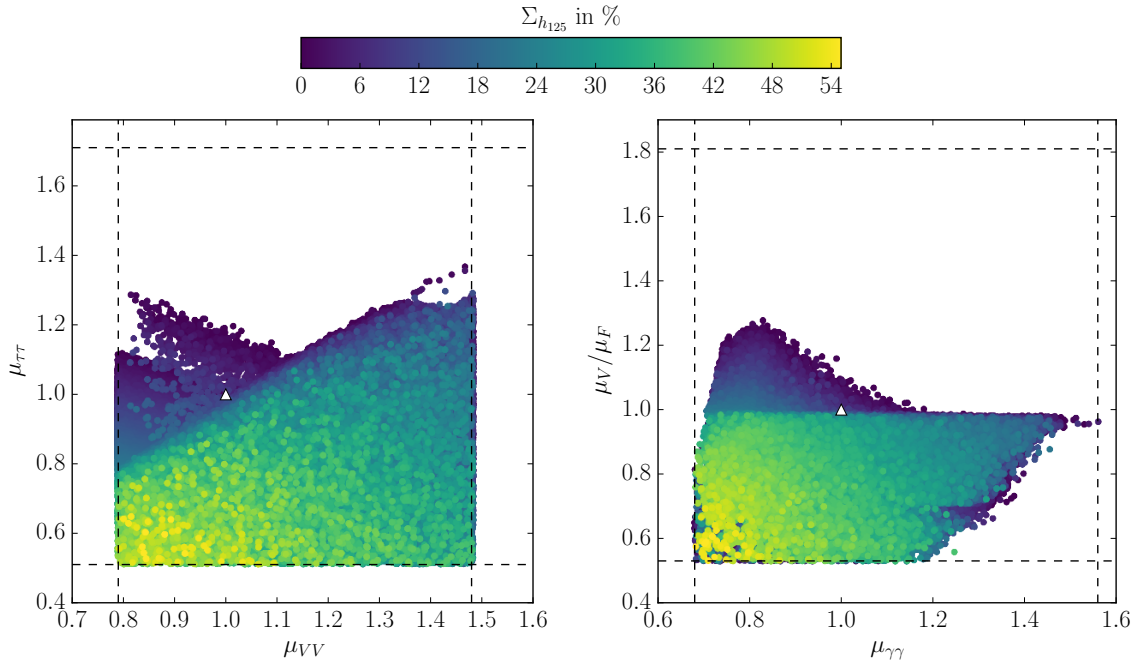

Figure 6. Type II: singlet admixture $\Sigma_{h_{125}}$ as a function of the most constraining signal strengths. The white triangle denotes the SM value.

leptons and b quarks, i.e. the spikes in figure 5 and figure 7 (left), respectively, where $\mu_{\tau\tau}$ reaches values of up to about 1.4. On the other hand, the effective coupling to gauge bosons cannot exceed one, so that overall the branching ratio into gauge boson is reduced in favor of BR($h_{125} \to \tau\tau$). Finally, the points with $\mu_{\tau\tau} > 1$ and $\mu_{VV} \approx 1$ are located in the wrong-sign regime and have reduced couplings to the gauge bosons. In figure 5 (right) these are the points below the dashed line and isolated from the bulk of the points. Figure 7 (right) shows the same coupling values squared, but now only for points in the wrong-sign limit, where the area with enhanced $\mu_{\tau\tau}$ can easily be identified. It is the resulting reduced decay width into VV that increases the branching ratio into $\tau\tau$ and thus $\mu_{\tau\tau}$. Note that in figure 5 (left) the sharp lines departing from the SM point to smaller and larger values of $c^2(h_{125}bb)$ are again due to the unitarity of the mixing matrix.

While the enhanced $\mu_{\tau\tau}$ is a feature of the 2HDM-like regions, singlet admixtures as large as 55% can be compatible with the current data. Interestingly the best measured quantities μ_{VV} and $\mu_{\gamma\gamma}$ are not the ones with the highest constraining power on the singlet admixtures. A value of $\mu_{VV} = 1$ still allows for $\Sigma_{h_{125}}$ of up to 50%, and a value of $\mu_{\gamma\gamma} = 1$ can be compatible with $\Sigma_{h_{125}}$ values of up to about 40%. A measurement of $\mu_{\tau\tau} \approx 1$ on the other hand constrains $\Sigma_{h_{125}}$ to be below about 25%. And a measurement of $\mu_V/\mu_F \geq 1$ enforces $\Sigma_{h_{125}} \lesssim 20\%$. This behaviour can be understood by inspecting the involved couplings individually. Overall, high singlet admixtures induce reduced couplings. However, figure 5 shows that the effective coupling to b-quarks is reduced more strongly than that to top-quarks, where the latter dominates gluon fusion production. Furthermore, among the physical points, a large singlet admixture leads to the effective gauge coupling

JHEP03(2017)094

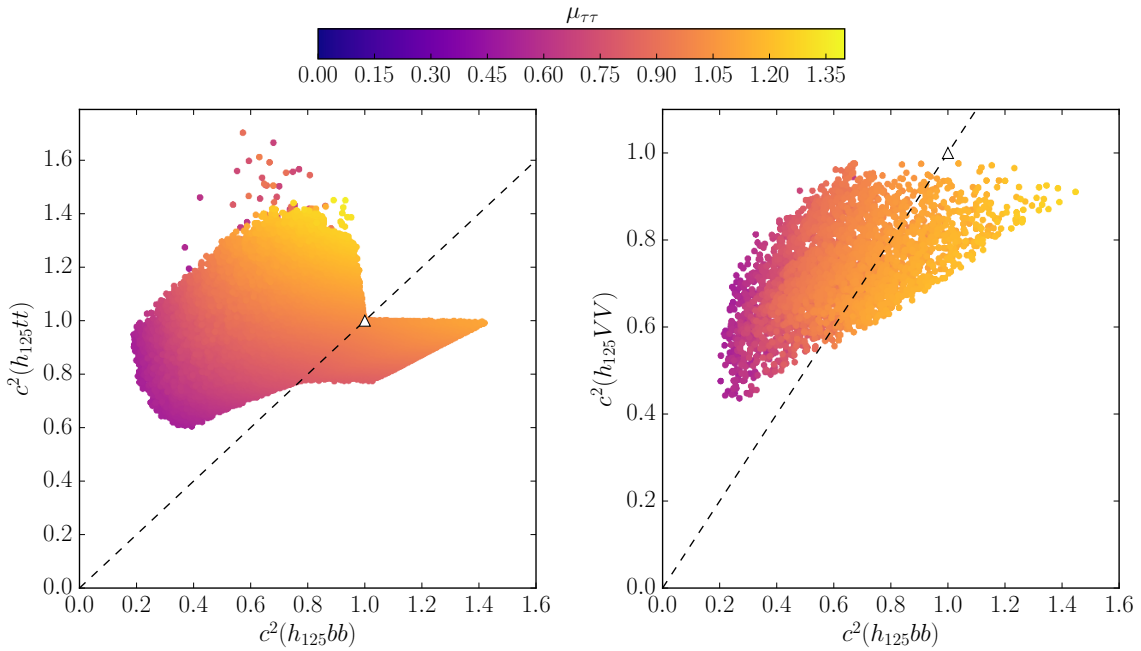

Figure 7. Type II: the $\tau\tau$ signal strength $\mu_{\tau\tau}$ as a function of the effective couplings squared. The white triangle denotes the SM value. The left plot shows only points in the correct-sign regime, the right plot only points in the wrong-sign regime. The dashed line respresents equal scaling of the couplings.

being larger than the effective bottom coupling. This means that the total width is reduced due to the strongly reduced $\Gamma(h_{125} \to b\bar{b})$, which dominates the total width in the SM case. In turn, this increases the BR$(h_{125} \to VV)$ and BR$(h_{125} \to \gamma\gamma)$ strongly enough to balance the reduced gluon fusion production cross section and the reduced partial widths in these channels, so that overall SM-values of μ_{VV} and $\mu_{\gamma\gamma}$ can be compatible with large singlet admixtures. The decay width into τ leptons, in contrast, gets rescaled by the same coupling as the $b\bar{b}$ channel in the type II model, so that the $\mu_{\tau\tau}$ is reduced for large singlet admixtures. Since with increasing singlet admixture $c(h_{125}VV)$ is more strongly reduced than $c(h_{125}tt)$ the value μ_V/μ_F is reduced for non-zero singlet admixtures. As the coupling to gauge bosons reaches at most 1, an enhanced μ_V/μ_F can only be due to a smaller coupling of h_{125} to tt. A value of $c(h_{125}VV)$ close to 1 with a simultaneously reduced $c(h_{125}tt)$ is only possible for small singlet admixtures. The corresponding bulge in figure 6 (right) contains points for which all other μ-values are close to their lower experimental boundaries. They are characterised by large couplings of the SM-like Higgs to a charged Higgs pair, which enters the loop-induced Higgs decay into photons and keeps $\mu_{\gamma\gamma}$ above its lower experimental boundary.

We conclude our discussion of the type II N2HDM by displaying in figure 8 the allowed N2HDM parameter region in the $\tan\beta$ versus $\Sigma_{h_{125}}$ plane (grey points) and its subsequent restriction by more precise measurements, with the same colour code as defined in eq. (5.3). It reflects our findings that the singlet admixture is most powerfully

JHEP03(2017)094

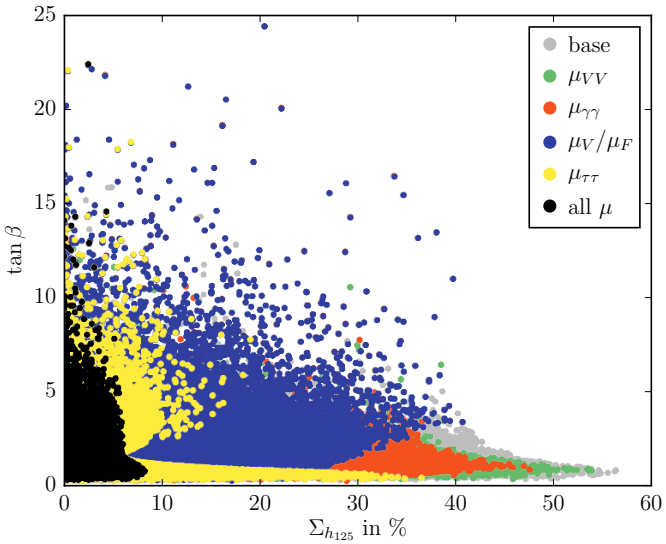

Figure 8. Type II: singlet admixture $\Sigma_{h_{125}}$ as a function of $\tan\beta$ and the precision in the μ-values. Grey points: all N2HDM scan parameter points; the remaining colors denote the μ values measured within 5% of the SM reference.

constrained by a precise measurement of $\mu_{\tau\tau}$ while being much less sensitive to the remaining μ-values. The restriction power depends on the value of $\tan\beta$. For medium values of $\tan\beta$ a singlet admixture of up to 20% is still compatible with a 5% measurement of $\mu_{\tau\tau}$ whereas for small values of $\tan\beta$ even up to 37% is allowed. Only the simultaneous measurement of all μ-values within 5% around the SM value restricts Σ to values below about 8%.

Type I N2HDM. We now turn to the discussion of the N2HDM type I. In this case the doublet Φ_2 couples to both up- and down-type quarks. Consequently, any change in the coupling to the top quark is induced also in the bottom quark coupling and vice versa. This restricts the available freedom in the choice of the parameters of the N2HDM so that, overall, less pronounced deviations from the SM or from the pure 2HDM are expected. This can be inferred from figures 9 and 10, which show, respectively, the singlet admixture of h_{125} as a function of the reduced signal strengths and the effective couplings. In constrast to the type II N2HDM the singlet admixture can reach at most 25%. Figure 9 shows the most constraining signal strenghts, i.e. $\mu_{\tau\tau}$ versus μ_{VV} in the left plot and μ_V/μ_F versus $\mu_{\gamma\gamma}$ in the right plot. From this figure it can be inferred that the allowed areas in these two planes are more reduced than in type II. While $\mu_{\gamma\gamma}$ is delimited by the present LHC data, only the lower bound of μ_{VV} is restricted due to the LHC fit value, while the upper μ_{VV} bound and the boundaries of $\mu_{\tau\tau}$ and μ_V/μ_F of the allowed areas are already well below the restrictions set by the LHC data. The highest singlet admixtures come with reduced signal strengths while the ratio $\mu_V/\mu_F \approx 1$. This is in accordance with figure 10, which shows the effective couplings squared, $c(h_{125}VV)^2$ versus $c^2(h_{125}bb)$ $(= c^2(h_{125}tt))$ together with the singlet admixture. Both effective couplings are reduced almost in parallel

JHEP03(2017)094

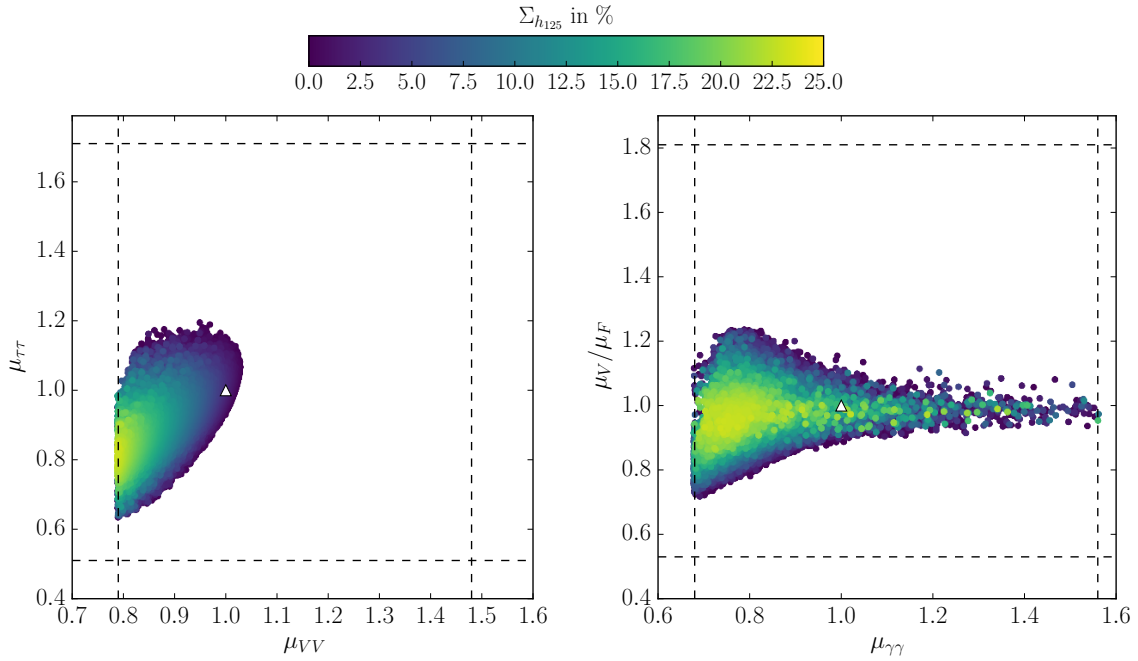

Figure 9. Type I: singlet admixture $\Sigma_{h_{125}}$ as a function of the most constraining signal strengths. The white triangle denotes the SM value.

with rising $\Sigma_{h_{125}}$ so that $\mu_V/\mu_F \sim c(h_{125}VV)^2/c(h_{125}ff)^2$ is close to one for large singlet admixtures.

The SM-like dark-blue boundary in figure 9 (left) with enhanced $\mu_{\tau\tau}$ corresponds to the right boundary of the area in figure 10 where $c^2(h_{125}bb)$ is enhanced and $c^2(h_{125}VV)$ is reduced. The simultaneous enhancement of the Higgs coupling to the bottom quarks and τ leptons leaves the branching ratio into τ's unchanged, but the enhanced Higgs couplings to fermions enhance the main production mechanism so that overall $\mu_{\tau\tau}$ is enhanced. Applying the same reasoning it is clear that the dark-blue boundary with reduced $\mu_{\tau\tau}$ values corresponds to the left dark-blue boundary in figure 10. This is also the area in figure 9 (right) corresponding to enhanced μ_V/μ_F values for $\mu_{\gamma\gamma} \lesssim 1.3$ in the 2HDM-like region (blue area). The reduced coupling to the bottom quarks reduces the dominating decay into $b\bar{b}$. The stronger reduction of $c(h_{125}bb)$ as compared to $c(h_{125}VV)$ overcompensates the reduced $\Gamma(h_{125} \to VV)$ so that overall $\mathrm{BR}(h_{125} \to VV)$ is enhanced and makes up for the reduction of the production cross section due to the smaller couplings to fermions. Simultaneously, this also ensures that μ_V/μ_F is enhanced. An analogous reasoning allows to identify the dark blue lower μ_V/μ_F values for $\mu_{\gamma\gamma} \lesssim 1.3$ with the right boundary in figure 10.

Figure 11 allows to analyse by which measurement the singlet admixture can be most effectively constrained. The colour code has been defined in eq. (5.3). As can already be inferred from figure 9 the singlet admixture is mostly restricted by the precise measurement of μ_{ZZ}, down to about 7.5% for a 5% accuracy in μ_{ZZ}. The simultaneous measurement of all μ-values with a precision of 5% hardly improves on this constraint. When comparing

JHEP03(2017)094

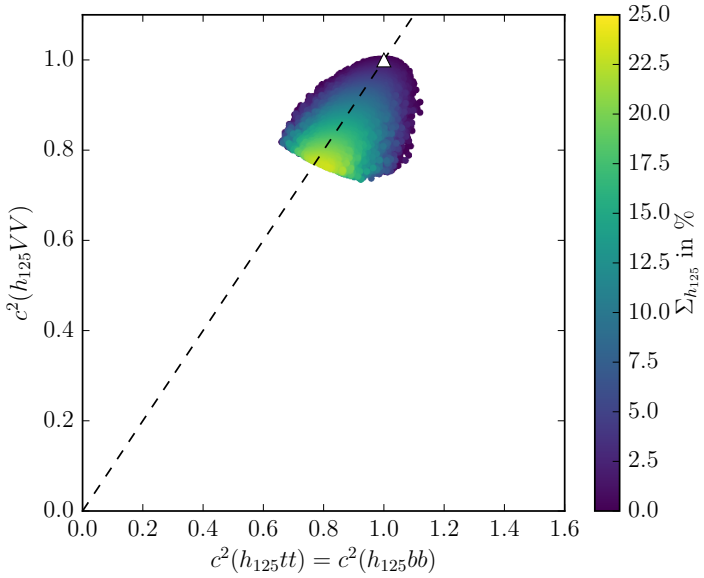

Figure 10. Type I: singlet admixture $\Sigma_{h_{125}}$ as a function of the effective couplings squared. The white triangle denotes the SM value. The dashed line respresents equal scaling of the couplings.

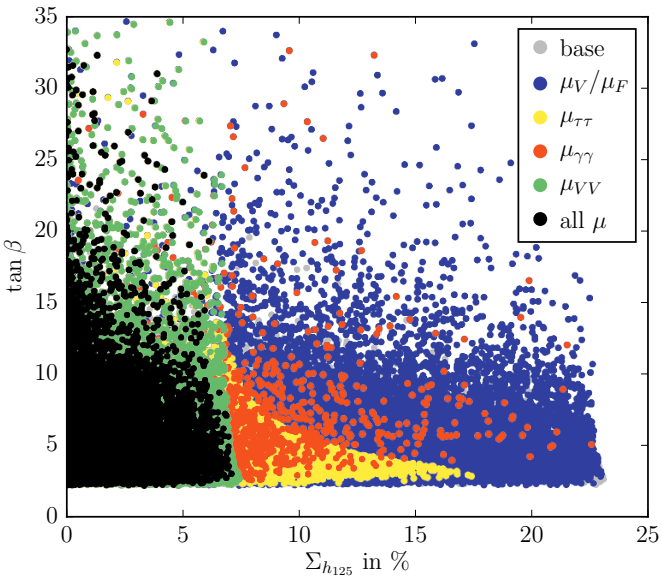

Figure 11. Type I: singlet admixture $\Sigma_{h_{125}}$ as a function of $\tan\beta$ and the precision in the μ-values. Grey points: all N2HDM scan parameter points; the remaining colors denote the μ values measured within 5% of the SM reference.

with the type II case, we can conclude that the structure of the Yukawa couplings decides which final state in the Higgs data is the most effective one in constraining the N2HDM, i.e. its singlet admixture.

JHEP03(2017)094

6 Conclusions

In this paper we have investigated the N2HDM, which is based on the CP-conserving 2HDM extended by a real scalar singlet field. It combines a parameter space which is larger than the 2HDM with a greater freedom in the choice of the parameters (compared to singlet extended supersymmetric models as e.g. the next-to-minimal supersymmetric model). This allows for an interesting phenomenology that is still compatible with the experimental data. Thus the Higgs couplings can carry a substantial singlet admixture. However, in order to be able to determine the allowed parameter space and thereby perform meaningful phenomenological analyses, the investigation of the constraints on the model had to be put on solid ground. In this paper we have performed a thorough analysis of the theoretical constraints on the N2HDM Higgs potential. First, we have collected from the literature the formulae for the N2HDM that test tree-level perturbative unitarity and stability of the vacuum. Moreover, for the first time, we have presented a detailed analysis of all the stationary points of the potential to obtain its global minimum. The model, together with the theoretical constraints, has been implemented in `ScannerS`. For the test of the experimental constraints the necessary branching ratios were obtained with the new program `N2HDECAY`. We have written this code based on `HDECAY` to provide the N2HDM branching ratios and total widths including the state-of-the-art higher order QCD corrections and off-shell decays. With these preparatory works completed we were then in the position to subject the N2HDM to critical theoretical and experimental scrutiny in the second part of the article.

Taking into account the theoretical and experimental constraints in the N2HDM, we performed a parameter space scan and analysed the properties of the allowed regions. In the type II N2HDM substantial singlet admixtures of up to 55% were found to be compatible with the data. It turned out that the most precisely measured quantities, μ_{VV} and $\mu_{\gamma\gamma}$, are not the most effective ones in constraining the singlet admixture, but instead it is the $\mu_{\tau\tau}$ observable. In the type I N2HDM, on the other hand, the parameter space is more constrained due to the universal fermion coupling to up- and down-type quarks and hence the allowed singlet admixture remains below about 25%. In the future, in this case, the singlet admixture will be most strongly constrained by the precise measurement of μ_{ZZ}.

Like in the 2HDM we find a wrong-sign regime in the N2HDM. While overall the allowed parameter space is larger in the N2HDM compared to the 2HDM, the wrong-sign regimes in both models are comparable. In this regime μ_V/μ_F is found to be well below 1, so that a measurement of a value near 1 excludes this scenario. Moreover, a future measurement of μ_{VV} with a precision of 5% around the SM value and the observation of $\mu_{\gamma\gamma} \gtrsim 0.9$ eliminates the wrong-sign regime. These findings are consistent with the observations in the 2HDM.

With the analysis tools provided in this study, the next natural step would be to compare the N2HDM with other extended Higgs sectors with a similar theoretical structure and Higgs spectrum, to investigate which observables allow to distinguish (or to exclude) the models.

JHEP03(2017)094

Acknowledgments

The authors acknowledge financial support from the DAAD project "PPP Portugal 2015" (ID: 57128671). M.S. was funded by FCT through the grant SFRH/BPD/69971/2010. The work in this paper was also supported by the CIDMA project UID/MAT/04106/2013. We are grateful to Michael Spira for useful comments. We acknowledge discussions with Pedro Ferreira.

A N2HDM parameters and self-couplings

In the following we give the transformation formulae between the N2HDM basis of the Lagrangian parameters and the physical basis defined in eq. (2.18). In A.2 we give the trilinear self-couplings in terms of the parameters of the physical basis.

A.1 Basis change

With the definition of

$$\tilde{\mu}^2 = \frac{m_{12}^2}{s_\beta c_\beta} \tag{A.1}$$

the quartic couplings λ_i of the N2HDM potential can be written in terms of the parameters of the physical basis as

$$\lambda_1 = \frac{1}{v^2 c_\beta^2}\left(- \tilde{\mu}^2 s_\beta^2 + \sum_{i=1}^{3} m_{H_i}^2 R_{i1}^2 \right) \tag{A.2}$$

$$\lambda_2 = \frac{1}{v^2 s_\beta^2}\left(- \tilde{\mu}^2 c_\beta^2 + \sum_{i=1}^{3} m_{H_i}^2 R_{i2}^2 \right) \tag{A.3}$$

$$\lambda_3 = \frac{1}{v^2}\left(- \tilde{\mu}^2 + \frac{1}{s_\beta c_\beta} \sum_{i=1}^{3} m_{H_i}^2 R_{i1} R_{i2} + 2 m_{H^\pm}^2 \right) \tag{A.4}$$

$$\lambda_4 = \frac{1}{v^2}(\tilde{\mu}^2 + m_A^2 - 2 m_{H^\pm}^2) \tag{A.5}$$

$$\lambda_5 = \frac{1}{v^2}(\tilde{\mu}^2 - m_A^2) \tag{A.6}$$

$$\lambda_6 = \frac{1}{v_S^2} \sum_{i=1}^{3} m_{H_i}^2 R_{i3}^2 \tag{A.7}$$

$$\lambda_7 = \frac{1}{v v_S c_\beta} \sum_{i=1}^{3} m_{H_i}^2 R_{i1} R_{i3} \tag{A.8}$$

$$\lambda_8 = \frac{1}{v v_S s_\beta} \sum_{i=1}^{3} m_{H_i}^2 R_{i2} R_{i3} \,. \tag{A.9}$$

The matrix elements R_{ij} in terms of the mixing angles $\alpha_{1,2,3}$ have been defined in eq. (2.13).

JHEP03(2017)094

A.2 The trilinear Higgs self-couplings

The trilinear Higgs self-couplings are derived from the terms of the Higgs potential cubic in the Higgs fields. After rotation to the mass basis and using the relations eqs. (A.2) to (A.9) the Feynman rules for the trilinear Higgs self-couplings between the physical Higgs fields modulo a factor i can be cast into the form

$$g_{H_iAA} = \frac{1}{v}\left(-\tilde{\mu}^2\left[\frac{R_{i1}}{c_\beta}+\frac{R_{i2}}{s_\beta}\right]+m_{H_i}^2\left[\frac{R_{i1}s_\beta^2}{c_\beta}+\frac{R_{i2}c_\beta^2}{s_\beta}\right]+2m_A^2\left[R_{i1}c_\beta+R_{i2}s_\beta\right]\right) \tag{A.10}$$

$$g_{H_iH^\pm H^\mp} = \frac{1}{v}\left(-\tilde{\mu}^2\left[\frac{R_{i1}}{c_\beta}+\frac{R_{i2}}{s_\beta}\right]+m_{H_i}^2\left[\frac{R_{i1}s_\beta^2}{c_\beta}+\frac{R_{i2}c_\beta^2}{s_\beta}\right]+2m_{H^\pm}^2\left[R_{i1}c_\beta+R_{i2}s_\beta\right]\right) \tag{A.11}$$

$$\begin{aligned} g_{H_iH_iH_i} = \frac{3}{v}\Bigg(&-\tilde{\mu}^2\left[R_{i2}^2c_\beta\left(\frac{R_{i2}c_\beta}{s_\beta}-R_{i1}\right)+R_{i1}^2s_\beta\left(\frac{R_{i1}s_\beta}{c_\beta}-R_{i2}\right)\right] \\ &+\frac{m_{H_i}^2}{v_S}\left[R_{i3}^3v+R_{i2}^3\frac{v_S}{s_\beta}+R_{i1}^3\frac{v_S}{c_\beta}\right]\Bigg) \end{aligned} \tag{A.12}$$

$$\begin{aligned} g_{H_iH_iH_j} = \frac{1}{v}\Bigg(&-\frac{1}{2}\tilde{\mu}^2\left(\frac{R_{i2}}{s_\beta}-\frac{R_{i1}}{c_\beta}\right)\left(6R_{i2}R_{j2}+6R_{i3}R_{j3}s_\beta^2+\sum_k\epsilon_{ijk}R_{k3}s_{2\beta}\right) \\ &+\frac{2m_{H_i}^2+m_{H_j}^2}{v_S}\left[R_{i3}^2R_{j3}v+R_{i2}^2R_{j2}\frac{v_S}{s_\beta}+R_{i1}^2R_{j1}\frac{v_S}{c_\beta}\right]\Bigg) \end{aligned} \tag{A.13}$$

$$\begin{aligned} g_{H_1H_2H_3} = \frac{1}{v}\Bigg(&\tilde{\mu}^2\Big[(2R_{12}R_{13}+R_{32}R_{33})c_\beta+(R_{31}R_{33}-3R_{12}R_{23}R_{33}-R_{21}R_{23})s_\beta \\ &+3R_{12}R_{22}\left(\frac{R_{31}}{c_\beta}-\frac{R_{32}}{s_\beta}\right)+3R_{13}R_{23}R_{31}\frac{s_\beta^2}{c_\beta}\Big] \\ &+\frac{\sum_{i=1}^3 m_{H_i}^2}{v_S}\left[R_{13}R_{23}R_{33}v+R_{12}R_{22}R_{32}\frac{v_S}{s_\beta}-R_{11}(R_{22}R_{32}+R_{23}R_{33})\frac{v_S}{c_\beta}\right]\Bigg) \end{aligned} \tag{A.14}$$

where ϵ_{ijk} denotes the totally antisymmetric tensor with $\epsilon_{123}=1$. Note, that in eqs. (A.10) to (A.14) there is no summation over repeated indices. The sums of different powers of R_{ij} arise from simplifications that exploit the orthogonality of the mixing matrix. The employed formula reads

$$R_{ij} = (-1)^{i+j}\det(\not{R}_{ij})\,. \tag{A.15}$$

The matrix $\not{R}_{ij}$ is the submatrix formed by deleting the i-th row and the j-th column from R. The indices i and j take any values in $\{1,2,3\}$.

B The Fortran code N2HDECAY

The code N2HDECAY is the N2HDM implementation in the program HDECAY, written in Fortran77. It is based on HDECAY v6.51. The code is completely self-contained. All changes related to the N2HDM have been implemented in the main file n2hdecay.f. Further linked routines have been taken over from the original HDECAY code. The implemented decay widths include the most important state-of-the-art higher order QCD corrections and the important off-shell decays. They can be taken over from the SM and the minimal

JHEP03(2017)094

supersymmetric extension (MSSM), respectively, for which HDECAY was originally designed. The electroweak corrections have been consistently turned off as they cannot be taken over from the available corrections in the SM and/or MSSM.

The N2HDM input parameters are specified in the input file n2hdecay.in. It is based on the extension of the input file hdecay.in. By setting the input value N2HDM= 1 in n2hdecay.in the user chooses to calculate the N2HDM branching ratios and total widths. The N2HDM-specific input parameters in the physical basis are then set in the blocks '2 Higgs Doublet Model' and 'N2HDM'. In the first block the user has to set PARAM=1 and can choose the TYPE of the fermion sector symmetry. Furthermore, the parameters $\tan\beta$ and m_{12}^2 and the pseudoscalar and charged Higgs masses are set here. In the N2HDM block the neutral Higgs masses, the mixing angles and the VEV of the singlet are set. We display part of an example input file relevant for the N2HDM. The gray lines contain parameters not used in the N2HDM.

```
N2HDM    = 1
...
************************* 2 Higgs Doublet Model *************************
  TYPE: 1 (I), 2 (II), 3 (lepton-specific), 4 (flipped)
  PARAM: 1 (masses), 2 (lambda_i)

PARAM    = 1
TYPE     = 2
********************
TGBET2HDM = 1.17639226D0
M_12^2    = 3.28390121D5
******************** PARAM=1:
ALPHA_H  = 10.D0
MHL      = 10.D0
MHH      = 10.D0
MHA      = 9.02919728D2
MH+-     = 8.59398112D2
******************** PARAM=2:
LAMBDA1  = 0D0
LAMBDA2  = 0D0
LAMBDA3  = 0D0
LAMBDA4  = 0D0
LAMBDA5  = 0D0
*************************** N2HDM ***********************************
*** needs TYPE, TGBET2HDM, M12Ĥ2, MHA and MH+- from the 2HDM block ***
MH1      = 1.25090000D2
MH2      = 8.17422761D2
MH3      = 9.76339405D2
alpha1   = 0.79503834
alpha2   = 0.13549279
alpha3   = 1.46729273
V_SING   = 1.49629673D3
*********************************************************************
...
```


JHEP03(2017)094

The code is compiled with the `makefile` by typing `make`. This produces an executable file called `run`. Typing `run` executes the program, which calculates the branching ratios and total widths that are written out together with the mass of the decaying Higgs boson. The output files are called `br.X_N2HDM_y`. Here `X=H1, H2, H3, A, H+` denotes the decaying Higgs particle. Files with the suffix `y=a` contain the branching ratios into fermions, with `y=b` the ones into gauge bosons and the ones with `y=c, d` the branching ratios into lighter Higgs pairs or a Higgs-gauge boson final state. In the following we present the example of an output file as obtained from the above input file. The produced output in the four output files `br.H3_N2HDM_y` for the heaviest neutral Higgs boson is given by

```
   MH3       BB          TAU TAU     MU MU       SS          CC          TT
-------------------------------------------------------------------------------
 976.339     0.3458E-03 0.5450E-04 0.1927E-06 0.1259E-06 0.1267E-04 0.8026

   MH3       GG          GAM GAM     Z GAM       WW          ZZ
-------------------------------------------------------------------------------
 976.339     0.1326E-02 0.3417E-05 0.6717E-06 0.4762E-01 0.2350E-01

   MH3       H1H1        H1H2        H2H2        AA          ZA
-------------------------------------------------------------------------------
 976.339     0.6375E-01 0.2923E-03 0.000       0.9115E-13 0.7821E-04

   MH3       W+- H-+     H+ H-       WIDTH
-------------------------------------------------------------------------------
 976.339     0.6038E-01 0.000       43.40
```

All files necessary for the program can be downloaded at the url:
http://www.itp.kit.edu/∼maggie/N2HDECAY/.
The webpage contains a short explanation of the program and information on updates and modifications of the program. Furthermore, sample output files can be found for a given input.

C Global minimum conditions

We start by recalling that, up to gauge symmetries, the most general constant field configuration, where all fields are real, is

$$\langle \Phi_1 \rangle = \begin{pmatrix} 0 \\ v_1 \end{pmatrix}, \qquad \langle \Phi_2 \rangle = \begin{pmatrix} v_{\rm cb} \\ v_2 + i v_{\rm cp} \end{pmatrix}, \qquad \langle \Phi_S \rangle = v_S \,. \tag{C.1}$$

The subscripts cp and cb refer to the case where CP or charge are spontaneously broken in scenarios where also both v_1 and v_2 are non-zero. In the case where only $v_{\rm cp}$ and/or $v_{\rm cb}$ are non-zero there is in fact no CP or charge breaking. One way to see this is by noting that such a configuration is continuously connected by a gauge transformation to the case where only $v_2 \neq 0$ (where it is more clear that there is no CP or charge breaking). Such a gauge transformation amounts to a redefinition of the charge operator by a rotation.

JHEP03(2017)094

In order to find all possible minima we consider the stationarity conditions for the VEVs,

$$\left\langle \frac{\partial V}{\partial v_1} \right\rangle = 0 \;\Leftrightarrow\; v_2 m_{12}^2 - v_1 m_{11}^2 = \frac{1}{2} v_1 (v_1^2 \lambda_1 + v_2^2 \lambda_{345} + v_{\mathrm{cb}}^2 \lambda_3 + v_{\mathrm{cp}}^2 \lambda_{34-5} + v_S^2 \lambda_7) \tag{C.2}$$

$$\left\langle \frac{\partial V}{\partial v_2} \right\rangle = 0 \;\Leftrightarrow\; v_1 m_{12}^2 - v_2 m_{22}^2 = \frac{1}{2} v_2 (v_1^2 \lambda_{345} + v_2^2 \lambda_2 + v_{\mathrm{cb}}^2 \lambda_2 + v_{\mathrm{cp}}^2 \lambda_2 + v_S^2 \lambda_8) \tag{C.3}$$

$$\left\langle \frac{\partial V}{\partial v_{\mathrm{cb}}} \right\rangle = 0 \;\Leftrightarrow\; -v_{\mathrm{cb}} m_{22}^2 = \frac{1}{2} v_{\mathrm{cb}} (v_1^2 \lambda_3 + v_2^2 \lambda_2 + v_{\mathrm{cb}}^2 \lambda_2 + v_{\mathrm{cp}}^2 \lambda_2 + v_S^2 \lambda_8) \tag{C.4}$$

$$\left\langle \frac{\partial V}{\partial v_{\mathrm{cp}}} \right\rangle = 0 \;\Leftrightarrow\; -v_{\mathrm{cp}} m_{22}^2 = \frac{1}{2} v_{\mathrm{cp}} (v_1^2 \lambda_{34-5} + v_2^2 \lambda_2 + v_{\mathrm{cb}}^2 \lambda_2 + v_{\mathrm{cp}}^2 \lambda_2 + v_S^2 \lambda_8) \tag{C.5}$$

$$\left\langle \frac{\partial V}{\partial v_{\mathrm{S}}} \right\rangle = 0 \;\Leftrightarrow\; -v_{\mathrm{S}} m_S^2 = \frac{1}{2} v_{\mathrm{S}} (v_1^2 \lambda_7 + v_2^2 \lambda_8 + v_{\mathrm{cb}}^2 \lambda_8 + v_{\mathrm{cp}}^2 \lambda_8 + v_S^2 \lambda_6)\,, \tag{C.6}$$

where λ_{345} has been defined in eq. (2.8) and

$$\lambda_{34-5} \equiv \lambda_3 + \lambda_4 - \lambda_5\,. \tag{C.7}$$

The derivatives with respect to the degrees of freedom, which have been removed through a gauge transformation in eq. (C.1), contribute with three further conditions

$$0 = v_1 v_2 v_{\mathrm{cb}} (\lambda_4 + \lambda_5 - 2 m_{12}^2) \tag{C.8}$$

$$0 = v_1 v_{\mathrm{cb}} v_{\mathrm{cp}} (\lambda_4 - \lambda_5) \tag{C.9}$$

$$0 = v_1 v_2 v_{\mathrm{cp}} (\lambda_5 - m_{12}^2)\,. \tag{C.10}$$

From eqs. (C.4) and (C.5) we infer that except for the special case

$$\lambda_4 = \lambda_5 \tag{C.11}$$

the VEVs v_{cb} and v_{cp} cannot be simultaneously non-zero. Eq. (C.9) is therefore always trivially satisfied. From eqs. (C.2) and (C.3) we conclude that

$$(v_1 = 0 \;\Leftrightarrow\; v_2 = 0) \;\vee\; m_{12}^2 = 0\,. \tag{C.12}$$

We further observe from eqs. (C.8) and (C.10) that

$$v_1 = v_2 = 0 \;\Rightarrow\; (v_{\mathrm{cb}} = v_{\mathrm{cp}} = 0 \;\vee\; m_{12}^2 = 0)\,. \tag{C.13}$$

The configurations forbidden by non-vanishing m_{12}^2 are inert stationary points where the whole doublet VEV can be brought into one Higgs doublet through a basis transformation. Models with inert Higgs doublets show a very different phenomenology and we only consider points with

$$|m_{12}^2| > 0\,. \tag{C.14}$$

In this case v_1 and v_2 are either both non-zero or v_S is the only non-vanishing VEV. All corresponding possible combinations of VEVs, i.e. all possible stationary points, are listed in table 7. The global minimum is given by the stationary point that leads to the smallest

JHEP03(2017)094

Case	I	IIa	IIb	sI	sIIa	sIIb	s
v_1	1	1	1	1	1	1	0
v_2	1	1	1	1	1	1	0
$v_{\rm cp}$	0	1	0	0	1	0	0
$v_{\rm cb}$	0	0	1	0	0	1	0
v_S	0	0	0	1	1	1	1

Table 7. All possible cases of VEVs being zero (0) or non-zero (1). Cases that are allowed only when specific parameter configurations hold, are not shown.

value for the scalar potential V. Since we have defined the field configurations eq. (C.1) such that the VEVs v_1, v_2, $v_{\rm cp}$ and $v_{\rm cb}$ are real, only solutions of the stationarity conditions with all VEVs squared positive are allowed. In the following we will provide the values of the scalar potential at all the stationary points listed in table 7. These stationary points need only be considered if the corresponding positivity conditions on the VEVs squared are satisfied.

C.1 2HDM-like stationary points

The three cases of the 2HDM-like stationary points are obtained setting $v_S = 0$. These are the stationary points of a 2HDM potential with the same parameters m_{11}^2, m_{22}^2, m_{12}^2 and λ_{1-5}.

Case I. This case with a CP and charge conserving minimum is the most complicated one. We start by rewriting the minimum conditions in terms of

$$v_1 = v\cos\delta \quad \text{and} \quad v_2 = v\sin\delta\,. \tag{C.15}$$

Without loss of generality all VEVs except v_2 can be chosen positive due to the $\mathbb{Z}_2$ symmetry. The convention $v_1 > 0$ implies

$$-\frac{\pi}{2} < \delta < \frac{\pi}{2}\,. \tag{C.16}$$

The resulting system of equations is used to eliminate v leading to a single quartic equation for $\sin^2\delta$,

$$\begin{aligned}
0 = {}& (m_{12}^2)^2\lambda_1^2 \\
&+ \sin^2\delta\big[-(m_{11}^2\lambda_{345} - m_{22}^2\lambda_1)^2 - 4(m_{12}^2)^2\lambda_1^2\big] \\
&+ (\sin^2\delta)^2\big[3(m_{11}^2\lambda_{345} - m_{22}^2\lambda_1)^2 + 2(m_{11}^2\lambda_{345} - m_{22}^2\lambda_1)(m_{22}^2\lambda_{345} - m_{11}^2\lambda_2) \\
&\qquad + 2(m_{12}^2)^2(3\lambda_1^2 - \lambda_1\lambda_2)\big] \\
&+ (\sin^2\delta)^3\big[-3(m_{11}^2\lambda_{345} - m_{22}^2\lambda_1)^2 + 4(m_{12}^2)^2\lambda_1(\lambda_2 - \lambda_1) \\
&\qquad - (m_{22}^2\lambda_{345} - m_{11}^2\lambda_2)\big((4m_{11}^2 + m_{22}^2)\lambda_{345} - 4m_{22}^2\lambda_1 - m_{11}^2\lambda_2\big)\big] \\
&+ (\sin^2\delta)^4\big[\big(m_{22}^2(\lambda_1 - \lambda_{345}) + m_{11}^2(\lambda_2 - \lambda_{345})\big)^2 \\
&\qquad + (m_{12}^2)^2(\lambda_1 - \lambda_2)^2\big]\,.
\end{aligned} \tag{C.17}$$

JHEP03(2017)094

Among the four solutions of eq. (C.17) for $\sin^2\delta$, which can be obtained numerically, only those are allowed that are real and in the open interval $(0,1)$. Reality for δ is required so that v_1 and v_2 are real. Each of these solutions leads to two possible values for v^2,

$$v^2 = \frac{2\left(m_{22}^2 \mp m_{12}^2\sqrt{\frac{1}{\sin^2\delta}-1}\right)}{\lambda_{345}(\sin^2\delta-1)-\lambda_2\sin^2\delta}\,. \tag{C.18}$$

The $\mp$ signs correspond to the two possible signs of $\sin\delta$ in the interval eq. (C.16). The values for v_1 and v_2 are then obtained from eq. (C.15) where both possible signs of v_2 need to be considered. Altogether this yields up to 16 possible solutions for v_1 and v_2 given by the four solutions for $\sin^2\delta$ times two for the sign of $\sin\delta$ times two for the sign of v_2. It should be noted only two of these solutions are independent as shown in [102, 103].

Case II. The system of minimum conditions obtained here can be solved analytically both for case IIa and IIb. The formula for the value of the potential at these points can be cast into the form

$$V(\mathrm{II}) = \frac{(m_{11}^2)^2\lambda_2 - 2m_{11}^2m_{22}^2x + (m_{22}^2)^2\lambda_1}{2\Lambda_{12}^{xx}} - \frac{(m_{12}^2)^2}{\lambda_{345}-x}\,, \tag{C.19}$$

where

$$x = \begin{cases} \lambda_{34-5} & \text{in case IIa} \\ \lambda_3 & \text{in case IIb} \end{cases} \tag{C.20}$$

and

$$\Lambda_{kl}^{ij} \equiv \lambda_i\lambda_j - \lambda_k\lambda_l\,. \tag{C.21}$$

Simultaneously the positivity conditions for the squared VEVs have to be fulfilled. They read

$$0 < v_{\mathrm{cb}}^2 \text{ or } v_{\mathrm{cp}}^2 = \frac{2(m_{12}^2)^2\Lambda_{12}^{xx}}{(\lambda_{345}-x)^2(m_{22}^2x - m_{11}^2\lambda_2)} + \frac{2(m_{22}^2\lambda_1 - m_{11}^2x)}{\Lambda_{12}^{xx}} \tag{C.22}$$

$$0 < v_1^2 = \frac{2(m_{11}^2\lambda_2 - m_{22}^2x)}{\Lambda_{12}^{xx}}\,. \tag{C.23}$$

Positivity of v_2^2 is guaranteed if v_1^2 is positive.

Special case $\boldsymbol{\lambda_4 = \lambda_5}$, $\boldsymbol{v_S = 0}$. In this special case v_{cb} and v_{cp} can be simultaneously non-zero. This is only possible if v_1 and v_2 are also non-zero. The resulting stationary value is

$$V(\lambda_4 = \lambda_5, v_S = 0) = -\frac{(m_{12}^2)^2}{2\lambda_4} + \frac{m_{11}^2\lambda_2 + m_{22}^2\lambda_1 - 2m_{11}^2m_{22}^2\lambda_3}{\Lambda_{12}^{33}}\,. \tag{C.24}$$

This value is obtained on a ring of constant $v_{\mathrm{cp}}^2 + v_{\mathrm{cb}}^2$. The positivity conditions therefore read

$$0 < v_{\mathrm{cb}}^2 + v_{\mathrm{cp}}^2 = -\frac{(m_{12}^2)^2\Lambda_{12}^{33}}{2(m_{11}^2\lambda_2 - m_{22}^2\lambda_3)\lambda_4^2} - \frac{2(m_{11}^2\lambda_3 - m_{22}^2\lambda_1)}{\Lambda_{12}^{33}} \tag{C.25}$$

$$0 < v_1^2 = \frac{2(m_{11}^2\lambda_2 - m_{22}^2\lambda_3)}{\Lambda_{12}^{33}}\,. \tag{C.26}$$

JHEP03(2017)094

C.2 Stationary points with a singlet VEV

The stationary points for a non-vanishing singlet VEV $v_S \neq 0$, as possible in the N2HDM, are obtained analogously to the previous cases.

Case sI. Again the case with non-vanishing v_1 and v_2 but zero $v_{\rm cp}$ and $v_{\rm cb}$ is the most complicated one and leads to a quartic equation for $\sin^2\delta$, with δ defined in eq. (C.15). It reads

$$\begin{aligned}
0 = {} & (m_{12}^2)^2(\Lambda_{16}^{77})^2 \\
& + \sin^2\delta\big[-\big((m_{11}^2\lambda_6 - m_S^2\lambda_7)\lambda_{345} + m_{22}^2\Lambda_{16}^{77} + (m_S^2\lambda_1 - m_{11}^2\lambda_7)\lambda_8\big)^2 - 4(m_{12}^2)^2(\Lambda_{16}^{77})^2\big] \\
& + (\sin^2\delta)^2\Big[\big((m_{11}^2\lambda_6 - m_S^2\lambda_7)\lambda_{345} - m_{11}^2\lambda_7\lambda_8 + m_{22}^2\Lambda_{16}^{77} + m_S^2\lambda_1\lambda_8\big) \\
& \qquad \times\Big(\big(3m_{11}^2\lambda_6 + 2m_{22}^2\lambda_6 - m_S^2(3\lambda_7 + 2\lambda_8)\big)\lambda_{345} + m_{11}^2(2\Lambda_{26}^{88} - 3\lambda_7\lambda_8) \\
& \qquad\quad + m_{22}^2(3\Lambda_{16}^{77} - 2\lambda_7\lambda_8) + m_S^2(2\lambda_2\lambda_7 + 3\lambda_1\lambda_8)\Big) + 2(m_{12}^2)^2\Lambda_{16}^{77}(3\Lambda_{16}^{77} - \Lambda_{26}^{88})\Big] \\
& + (\sin^2\delta)^3\Big[\Big(\big(m_S^2(3\lambda_7 + \lambda_8) - (3m_{11}^2 + m_{22}^2)\lambda_6\big)\lambda_{345} + m_{11}^2(3\lambda_7\lambda_8 - \Lambda_{26}^{88}) \\
& \qquad + m_{22}^2(\lambda_7\lambda_8 - 3\Lambda_{16}^{77}) - m_S^2(\lambda_2\lambda_7 + 3\lambda_1\lambda_8)\Big) \\
& \qquad \times\Big(\big((m_{11}^2 + m_{22}^2)\lambda_6 - m_S^2(\lambda_7 + \lambda_8)\big)\lambda_{345} + m_{11}^2(\Lambda_{26}^{88} - \lambda_7\lambda_8) \\
& \qquad\quad + m_{22}^2(\Lambda_{16}^{77} - \lambda_7\lambda_8) + m_S^2(\lambda_2\lambda_7 + \lambda_1\lambda_8)\Big) + 4(m_{12}^2)^2\Lambda_{16}^{77}(\Lambda_{26}^{88} - \Lambda_{16}^{77})\Big] \\
& + (\sin^2\delta)^4\Big[\Big(\big((m_{11}^2 + m_{22}^2)\lambda_6 - m_S^2(\lambda_7 + \lambda_8)\big)\lambda_{345} + m_{11}^2(\Lambda_{26}^{88} - \lambda_7\lambda_8) \\
& \qquad + m_{22}^2(\Lambda_{16}^{77} - \lambda_7\lambda_8) + m_S^2(\lambda_2\lambda_7 + \lambda_1\lambda_8)\Big)^2 + (m_{12}^2)^2(\Lambda_{26}^{88} - \Lambda_{16}^{77})^2\Big] .
\end{aligned} \tag{C.27}$$

The real solutions for $\sin^2\delta$ in the open interval $(0,1)$ imply two possible values for v^2,

$$v^2 = \frac{2\lambda_6\Big(m_{22}^2 \mp m_{12}^2\sqrt{\frac{1}{\sin^2\delta} - 1}\Big) - 2m_S^2\lambda_8}{(\sin^2\delta - 1)(\lambda_6\lambda_{345} - \lambda_7\lambda_8) + \Lambda_{26}^{88}\sin^2\delta} , \tag{C.28}$$

depending on the sign of $\sin\delta$ in the interval. For v_S^2 we have

$$v_S^2 = -\frac{\lambda_7 v_1^2 + \lambda_8 v_2^2 + 2m_S^2}{\lambda_6} . \tag{C.29}$$

Valid solutions are given for positive values of v^2 and v_S^2. The sign of v_S is irrelevant so that also here we have up to 16 solutions and the corresponding values of the potential that can be obtained numerically.

Case sII. Defining again for the two subcases

$$x = \begin{cases} \lambda_{34-5} & \text{in case sIIa} \\ \lambda_3 & \text{in case sIIb} \end{cases} , \tag{C.30}$$

JHEP03(2017)094

we have the stationary values and positivity conditions for the case sII stationary point given by

$$V(\mathrm{sII}) = -\frac{(m_{12}^2)^2}{\lambda_{345}-x} + \frac{(m_{11}^2)^2\Lambda_{26}^{88} + (m_{22}^2)^2\Lambda_{16}^{77} + (m_S^2)^2\Lambda_{12}^{xx}}{2(\lambda_7\Lambda_{27}^{x8} + x\Lambda_{x6}^{78} - \lambda_1\Lambda_{26}^{88})} - \frac{m_{11}^2 m_{22}^2\Lambda_{x6}^{78} + m_{11}^2 m_S^2\Lambda_{27}^{x8} + m_{22}^2 m_S^2\Lambda_{18}^{x7}}{\lambda_7\Lambda_{27}^{x8} + x\Lambda_{x6}^{78} - \lambda_1\Lambda_{26}^{88}} \tag{C.31}$$

and

$$0 < v_{\mathrm{cb}}^2 \text{ or } v_{\mathrm{cp}}^2 = \frac{(m_{12}^2)^2(\lambda_7\Lambda_{27}^{x8} + x\Lambda_{x6}^{78} - \lambda_1\Lambda_{26}^{88})}{2(\lambda_{345}-x)^2(m_S^2\Lambda_{27}^{x8} + m_{22}^2\Lambda_{x6}^{78} - m_{11}^2\Lambda_{26}^{88})} + \frac{2m_{22}^2\Lambda_{16}^{77} - 2m_S^2\Lambda_{18}^{x7} - 2m_{11}^2\Lambda_{x6}^{78}}{\lambda_7\Lambda_{27}^{x8} + x\Lambda_{x6}^{78} - \lambda_1\Lambda_{26}^{88}} \tag{C.32}$$

$$0 < v_S^2 = \frac{2m_S^2\Lambda_{12}^{xx} - 2m_{11}^2\Lambda_{27}^{x8} - 2m_{22}^2\Lambda_{18}^{x7}}{\lambda_7\Lambda_{27}^{x8} + x\Lambda_{x6}^{78} - \lambda_1\Lambda_{26}^{88}} \tag{C.33}$$

$$0 < v_1^2 = \frac{-2m_S^2\Lambda_{27}^{x8} - 2m_{22}^2\Lambda_{x6}^{78} + 2m_{11}^2\Lambda_{26}^{88}}{\lambda_7\Lambda_{27}^{x8} + x\Lambda_{x6}^{78} - \lambda_1\Lambda_{26}^{88}}\,. \tag{C.34}$$

Positivity of v_2^2 is ensured if v_1^2 is positive.

Case s. For the case denoted by s the value of the potential at the stationary point simplifies to

$$V(\mathrm{s}) = -\frac{(m_S^2)^2}{2\lambda_6}\,, \tag{C.35}$$

which is a valid solution ($v_S^2 > 0$) if

$$m_S^2 < 0\,. \tag{C.36}$$

Special case $\boldsymbol{\lambda_4 = \lambda_5}$, $\boldsymbol{v_S \neq 0}$. If $\lambda_4 = \lambda_5$ all VEVs can be simultaneously non-zero. In this case the scalar potential takes the stationary value

$$V(\lambda_4 = \lambda_5, v_S \neq 0) = -\frac{(m_{12}^2)^2}{2\lambda_4} + \frac{(m_{11}^2)^2\Lambda_{26}^{88} + (m_{22}^2)^2\Lambda_{16}^{77} + (m_S^2)^2\Lambda_{12}^{33}}{2(\lambda_7\Lambda_{27}^{38} + \lambda_3\Lambda_{36}^{78} - \lambda_1\Lambda_{26}^{88})} - \frac{m_{11}^2 m_{22}^2\Lambda_{36}^{78} + m_{11}^2 m_S^2\Lambda_{27}^{38} + m_{22}^2 m_S^2\Lambda_{18}^{37}}{\lambda_7\Lambda_{27}^{38} + \lambda_3\Lambda_{36}^{78} - \lambda_1\Lambda_{26}^{88}}\,. \tag{C.37}$$

This stationary value is again obtained on a ring of constant $v_{\mathrm{cb}}^2 + v_{\mathrm{cp}}^2$. The corresponding positivity conditions read

$$0 < v_{\mathrm{cb}}^2 + v_{\mathrm{cp}}^2 = \frac{(m_{12}^2)^2(\lambda_7\Lambda_{27}^{38} + \lambda_3\Lambda_{36}^{78} - \lambda_1\Lambda_{26}^{88})}{2\lambda_4^2(m_S^2\Lambda_{27}^{38} + m_{22}^2\Lambda_{36}^{78} - m_{11}^2\Lambda_{26}^{88})} + \frac{2(m_{22}^2\Lambda_{16}^{77} - m_S^2\Lambda_{18}^{37} - m_{11}^2\Lambda_{36}^{78})}{\lambda_7\Lambda_{27}^{38} + \lambda_3\Lambda_{36}^{78} - \lambda_1\Lambda_{26}^{88}} \tag{C.38}$$

$$0 < v_S^2 = \frac{2(m_S^2\Lambda_{12}^{33} - m_{11}^2\Lambda_{27}^{38} - m_{22}^2\Lambda_{18}^{37})}{\lambda_7\Lambda_{27}^{38} + \lambda_3\Lambda_{36}^{78} - \lambda_1\Lambda_{26}^{88}} \tag{C.39}$$

$$0 < v_1^2 = -\frac{2(m_S^2\Lambda_{27}^{38} + m_{22}^2\Lambda_{36}^{78} - m_{11}^2\Lambda_{26}^{88})}{\lambda_7\Lambda_{27}^{38} + \lambda_3\Lambda_{36}^{78} - \lambda_1\Lambda_{26}^{88}}\,. \tag{C.40}$$

JHEP03(2017)094

In order to check if our minimum is the global one we compare the value of the scalar potential at our minimum with the values of the potential at all the stationary points listed above. In practice this means that we need to compare with the up to five different analytically known values of cases (s)II and case s and with the numerical solutions of case (s)I.

References

[1] ATLAS collaboration, *Observation of a new particle in the search for the standard model Higgs boson with the ATLAS detector at the LHC*, *Phys. Lett.* **B 716** (2012) 1 [arXiv:1207.7214] [INSPIRE].

[2] CMS collaboration, *Observation of a new boson at a mass of 125 GeV with the CMS experiment at the LHC*, *Phys. Lett.* **B 716** (2012) 30 [arXiv:1207.7235] [INSPIRE].

[3] C. Englert et al., *Precision measurements of Higgs couplings: implications for new physics scales*, *J. Phys.* **G 41** (2014) 113001 [arXiv:1403.7191] [INSPIRE].

[4] ATLAS and CMS collaborations, *Combined measurement of the Higgs boson mass in pp collisions at $\sqrt{s} = 7$ and 8 TeV with the ATLAS and CMS experiments*, *Phys. Rev. Lett.* **114** (2015) 191803 [arXiv:1503.07589] [INSPIRE].

[5] H. Terazawa, K. Akama and Y. Chikashige, *Unified model of the Nambu-Jona-Lasinio type for all elementary particle forces*, *Phys. Rev.* **D 15** (1977) 480 [INSPIRE].

[6] H. Terazawa, *Subquark model of leptons and quarks*, *Phys. Rev.* **D 22** (1980) 184 [INSPIRE].

[7] D.B. Kaplan and H. Georgi, SU(2) × U(1) *breaking by vacuum misalignment*, *Phys. Lett.* **B 136** (1984) 183 [INSPIRE].

[8] S. Dimopoulos and J. Preskill, *Massless composites with massive constituents*, *Nucl. Phys.* **B 199** (1982) 206 [INSPIRE].

[9] T. Banks, *Constraints on* SU(2) × U(1) *breaking by vacuum misalignment*, *Nucl. Phys.* **B 243** (1984) 125 [INSPIRE].

[10] D.B. Kaplan, H. Georgi and S. Dimopoulos, *Composite Higgs scalars*, *Phys. Lett.* **B 136** (1984) 187 [INSPIRE].

[11] H. Georgi, D.B. Kaplan and P. Galison, *Calculation of the composite Higgs mass*, *Phys. Lett.* **B 143** (1984) 152 [INSPIRE].

[12] H. Georgi and D.B. Kaplan, *Composite Higgs and custodial* SU(2), *Phys. Lett.* **B 145** (1984) 216 [INSPIRE].

[13] M.J. Dugan, H. Georgi and D.B. Kaplan, *Anatomy of a composite Higgs model*, *Nucl. Phys.* **B 254** (1985) 299 [INSPIRE].

[14] G.F. Giudice, C. Grojean, A. Pomarol and R. Rattazzi, *The strongly-interacting light Higgs*, *JHEP* **06** (2007) 045 [hep-ph/0703164] [INSPIRE].

[15] K. Agashe, R. Contino and A. Pomarol, *The minimal composite Higgs model*, *Nucl. Phys.* **B 719** (2005) 165 [hep-ph/0412089] [INSPIRE].

JHEP03(2017)094

[16] R. Contino, L. Da Rold and A. Pomarol, *Light custodians in natural composite Higgs models*, *Phys. Rev.* **D 75** (2007) 055014 [hep-ph/0612048] [INSPIRE].

[17] CMS collaboration, *Constraints on the spin-parity and anomalous HVV couplings of the Higgs boson in proton collisions at 7 and 8 TeV*, *Phys. Rev.* **D 92** (2015) 012004 [arXiv:1411.3441] [INSPIRE].

[18] ATLAS collaboration, *Study of the spin and parity of the Higgs boson in diboson decays with the ATLAS detector*, *Eur. Phys. J.* **C 75** (2015) 476 [arXiv:1506.05669] [INSPIRE].

[19] CMS collaboration, *Precise determination of the mass of the Higgs boson and tests of compatibility of its couplings with the standard model predictions using proton collisions at 7 and 8 TeV*, *Eur. Phys. J.* **C 75** (2015) 212 [arXiv:1412.8662] [INSPIRE].

[20] ATLAS collaboration, *Measurements of the Higgs boson production and decay rates and coupling strengths using pp collision data at $\sqrt{s} = 7$ and 8 TeV in the ATLAS experiment*, *Eur. Phys. J.* **C 76** (2016) 6 [arXiv:1507.04548] [INSPIRE].

[21] J.F. Gunion, H.E. Haber, G.L. Kane and S. Dawson, *The Higgs hunter's guide*, *Front. Phys.* **80** (2000) 1 [INSPIRE].

[22] T.D. Lee, *A theory of spontaneous T violation*, *Phys. Rev.* **D 8** (1973) 1226 [INSPIRE].

[23] G.C. Branco et al., *Theory and phenomenology of two-Higgs-doublet models*, *Phys. Rept.* **516** (2012) 1 [arXiv:1106.0034] [INSPIRE].

[24] X.-G. He, T. Li, X.-Q. Li, J. Tandean and H.-C. Tsai, *Constraints on scalar dark matter from direct experimental searches*, *Phys. Rev.* **D 79** (2009) 023521 [arXiv:0811.0658] [INSPIRE].

[25] B. Grzadkowski and P. Osland, *Tempered two-Higgs-doublet model*, *Phys. Rev.* **D 82** (2010) 125026 [arXiv:0910.4068] [INSPIRE].

[26] H.E. Logan, *Dark matter annihilation through a lepton-specific Higgs boson*, *Phys. Rev.* **D 83** (2011) 035022 [arXiv:1010.4214] [INSPIRE].

[27] M.S. Boucenna and S. Profumo, *Direct and indirect singlet scalar dark matter detection in the lepton-specific two-Higgs-doublet model*, *Phys. Rev.* **D 84** (2011) 055011 [arXiv:1106.3368] [INSPIRE].

[28] X.-G. He, B. Ren and J. Tandean, *Hints of standard model Higgs boson at the LHC and light dark matter searches*, *Phys. Rev.* **D 85** (2012) 093019 [arXiv:1112.6364] [INSPIRE].

[29] Y. Bai, V. Barger, L.L. Everett and G. Shaughnessy, *Two-Higgs-doublet-portal dark-matter model: LHC data and Fermi-LAT 135 GeV line*, *Phys. Rev.* **D 88** (2013) 015008 [arXiv:1212.5604] [INSPIRE].

[30] X.-G. He and J. Tandean, *Low-mass dark-matter hint from CDMS II, Higgs boson at the LHC and darkon models*, *Phys. Rev.* **D 88** (2013) 013020 [arXiv:1304.6058] [INSPIRE].

[31] Y. Cai and T. Li, *Singlet dark matter in a type-II two Higgs doublet model*, *Phys. Rev.* **D 88** (2013) 115004 [arXiv:1308.5346] [INSPIRE].

[32] J. Guo and Z. Kang, *Higgs naturalness and dark matter stability by scale invariance*, *Nucl. Phys.* **B 898** (2015) 415 [arXiv:1401.5609] [INSPIRE].

[33] L. Wang and X.-F. Han, *A simplified 2HDM with a scalar dark matter and the galactic center gamma-ray excess*, *Phys. Lett.* **B 739** (2014) 416 [arXiv:1406.3598] [INSPIRE].

JHEP03(2017)094

[34] A. Drozd, B. Grzadkowski, J.F. Gunion and Y. Jiang, *Extending two-Higgs-doublet models by a singlet scalar field — the case for dark matter*, *JHEP* **11** (2014) 105 [arXiv:1408.2106] [INSPIRE].

[35] R. Campbell, S. Godfrey, H.E. Logan, A.D. Peterson and A. Poulin, *Implications of the observation of dark matter self-interactions for singlet scalar dark matter*, *Phys. Rev.* **D 92** (2015) 055031 [arXiv:1505.01793] [INSPIRE].

[36] A. Drozd, B. Grzadkowski, J.F. Gunion and Y. Jiang, *Isospin-violating dark-matter-nucleon scattering via two-Higgs-doublet-model portals*, *JCAP* **10** (2016) 040 [arXiv:1510.07053] [INSPIRE].

[37] S. von Buddenbrock et al., *Phenomenological signatures of additional scalar bosons at the LHC*, *Eur. Phys. J.* **C 76** (2016) 580 [arXiv:1606.01674] [INSPIRE].

[38] C.-Y. Chen, M. Freid and M. Sher, *Next-to-minimal two Higgs doublet model*, *Phys. Rev.* **D 89** (2014) 075009 [arXiv:1312.3949] [INSPIRE].

[39] A. Djouadi, W. Kilian, M. Mühlleitner and P.M. Zerwas, *Testing Higgs self-couplings at e^+e^- linear colliders*, *Eur. Phys. J.* **C 10** (1999) 27 [hep-ph/9903229] [INSPIRE].

[40] A. Djouadi, W. Kilian, M. Mühlleitner and P.M. Zerwas, *Production of neutral Higgs boson pairs at LHC*, *Eur. Phys. J.* **C 10** (1999) 45 [hep-ph/9904287] [INSPIRE].

[41] M.M. Mühlleitner, *Higgs particles in the standard model and supersymmetric theories*, Ph.D. Thesis, Hamburg University (2000) [hep-ph/0008127] [INSPIRE].

[42] P. Fayet, *Supergauge invariant extension of the Higgs mechanism and a model for the electron and its neutrino*, *Nucl. Phys.* **B 90** (1975) 104 [INSPIRE].

[43] R. Barbieri, S. Ferrara and C.A. Savoy, *Gauge models with spontaneously broken local supersymmetry*, *Phys. Lett.* **B 119** (1982) 343 [INSPIRE].

[44] M. Dine, W. Fischler and M. Srednicki, *A simple solution to the strong CP problem with a harmless axion*, *Phys. Lett.* **B 104** (1981) 199 [INSPIRE].

[45] H.P. Nilles, M. Srednicki and D. Wyler, *Weak interaction breakdown induced by supergravity*, *Phys. Lett.* **B 120** (1983) 346 [INSPIRE].

[46] J.M. Frere, D.R.T. Jones and S. Raby, *Fermion masses and induction of the weak scale by supergravity*, *Nucl. Phys.* **B 222** (1983) 11 INSPIRE].

[47] J.P. Derendinger and C.A. Savoy, *Quantum effects and* SU(2) × U(1) *breaking in supergravity gauge theories*, *Nucl. Phys.* **B 237** (1984) 307 [INSPIRE].

[48] J.R. Ellis, J.F. Gunion, H.E. Haber, L. Roszkowski and F. Zwirner, *Higgs bosons in a nonminimal supersymmetric model*, *Phys. Rev.* **D 39** (1989) 844 [INSPIRE].

[49] M. Drees, *Supersymmetric models with extended Higgs sector*, *Int. J. Mod. Phys.* **A 4** (1989) 3635 [INSPIRE].

[50] U. Ellwanger, M. Rausch de Traubenberg and C.A. Savoy, *Particle spectrum in supersymmetric models with a gauge singlet*, *Phys. Lett.* **B 315** (1993) 331 [hep-ph/9307322] [INSPIRE].

[51] U. Ellwanger, M. Rausch de Traubenberg and C.A. Savoy, *Higgs phenomenology of the supersymmetric model with a gauge singlet*, *Z. Phys.* **C 67** (1995) 665 [hep-ph/9502206] [INSPIRE].

JHEP03(2017)094

[52] U. Ellwanger, M. Rausch de Traubenberg and C.A. Savoy, *Phenomenology of supersymmetric models with a singlet*, *Nucl. Phys.* **B 492** (1997) 21 [hep-ph/9611251] [INSPIRE].

[53] T. Elliott, S.F. King and P.L. White, *Unification constraints in the next-to-minimal supersymmetric standard model*, *Phys. Lett.* **B 351** (1995) 213 [hep-ph/9406303] [INSPIRE].

[54] S.F. King and P.L. White, *Resolving the constrained minimal and next-to-minimal supersymmetric standard models*, *Phys. Rev.* **D 52** (1995) 4183 [hep-ph/9505326] [INSPIRE].

[55] F. Franke and H. Fraas, *Neutralinos and Higgs bosons in the next-to-minimal supersymmetric standard model*, *Int. J. Mod. Phys.* **A 12** (1997) 479 [hep-ph/9512366] [INSPIRE].

[56] M. Maniatis, *The next-to-minimal supersymmetric extension of the standard model reviewed*, *Int. J. Mod. Phys.* **A 25** (2010) 3505 [arXiv:0906.0777] [INSPIRE].

[57] U. Ellwanger, C. Hugonie and A.M. Teixeira, *The next-to-minimal supersymmetric standard model*, *Phys. Rept.* **496** (2010) 1 [arXiv:0910.1785] [INSPIRE].

[58] H. Davoudiasl, R. Kitano, T. Li and H. Murayama, *The new minimal standard model*, *Phys. Lett.* **B 609** (2005) 117 [hep-ph/0405097] [INSPIRE].

[59] J.J. van der Bij, *The minimal non-minimal standard model*, *Phys. Lett.* **B 636** (2006) 56 [hep-ph/0603082] [INSPIRE].

[60] A. Datta and A. Raychaudhuri, *Next-to-minimal Higgs: mass bounds and search prospects*, *Phys. Rev.* **D 57** (1998) 2940 [hep-ph/9708444] [INSPIRE].

[61] R.M. Schabinger and J.D. Wells, *A minimal spontaneously broken hidden sector and its impact on Higgs boson physics at the Large Hadron Collider*, *Phys. Rev.* **D 72** (2005) 093007 [hep-ph/0509209] [INSPIRE].

[62] O. Bahat-Treidel, Y. Grossman and Y. Rozen, *Hiding the Higgs at the LHC*, *JHEP* **05** (2007) 022 [hep-ph/0611162] [INSPIRE].

[63] T. Robens and T. Stefaniak, *Status of the Higgs singlet extension of the standard model after LHC Run 1*, *Eur. Phys. J.* **C 75** (2015) 104 [arXiv:1501.02234] [INSPIRE].

[64] V. Barger, P. Langacker and G. Shaughnessy, *Collider signatures of singlet extended Higgs sectors*, *Phys. Rev.* **D 75** (2007) 055013 [hep-ph/0611239] [INSPIRE].

[65] V. Barger, P. Langacker, M. McCaskey, M.J. Ramsey-Musolf and G. Shaughnessy, *LHC phenomenology of an extended standard model with a real scalar singlet*, *Phys. Rev.* **D 77** (2008) 035005 [arXiv:0706.4311] [INSPIRE].

[66] V. Barger, P. Langacker, M. McCaskey, M. Ramsey-Musolf and G. Shaughnessy, *Complex singlet extension of the standard model*, *Phys. Rev.* **D 79** (2009) 015018 [arXiv:0811.0393] [INSPIRE].

[67] D. O'Connell, M.J. Ramsey-Musolf and M.B. Wise, *Minimal extension of the standard model scalar sector*, *Phys. Rev.* **D 75** (2007) 037701 [hep-ph/0611014] [INSPIRE].

[68] R.S. Gupta and J.D. Wells, *Higgs boson search significance deformations due to mixed-in scalars*, *Phys. Lett.* **B 710** (2012) 154 [arXiv:1110.0824] [INSPIRE].

[69] A. Ahriche, A. Arhrib and S. Nasri, *Higgs phenomenology in the two-singlet model*, *JHEP* **02** (2014) 042 [arXiv:1309.5615] [INSPIRE].

JHEP03(2017)094

[70] R. Coimbra, M.O.P. Sampaio and R. Santos, *ScannerS: constraining the phase diagram of a complex scalar singlet at the LHC*, *Eur. Phys. J.* **C 73** (2013) 2428 [arXiv:1301.2599] [INSPIRE].

[71] C.-Y. Chen, S. Dawson and I.M. Lewis, *Exploring resonant di-Higgs boson production in the Higgs singlet model*, *Phys. Rev.* **D 91** (2015) 035015 [arXiv:1410.5488] [INSPIRE].

[72] S. Profumo, M.J. Ramsey-Musolf, C.L. Wainwright and P. Winslow, *Singlet-catalyzed electroweak phase transitions and precision Higgs boson studies*, *Phys. Rev.* **D 91** (2015) 035018 [arXiv:1407.5342] [INSPIRE].

[73] R. Costa, A.P. Morais, M.O.P. Sampaio and R. Santos, *Two-loop stability of a complex singlet extended standard model*, *Phys. Rev.* **D 92** (2015) 025024 [arXiv:1411.4048] [INSPIRE].

[74] R. Costa, M. Mühlleitner, M.O.P. Sampaio and R. Santos, *Singlet extensions of the standard model at LHC Run 2: benchmarks and comparison with the NMSSM*, *JHEP* **06** (2016) 034 [arXiv:1512.05355] [INSPIRE].

[75] J. Wittbrodt, *Phenomenological comparison of models with extended Higgs sectors*, Master Thesis, Karlsruhe Institute of Technology (2016).

[76] A. Djouadi, J. Kalinowski and M. Spira, *HDECAY: a program for Higgs boson decays in the standard model and its supersymmetric extension*, *Comput. Phys. Commun.* **108** (1998) 56 [hep-ph/9704448] [INSPIRE].

[77] J.M. Butterworth et al., *The Tools and Monte Carlo Working Group summary report from the Les Houches 2009 workshop on TeV Colliders*, in Proceedings of the *6th Les Houches Workshop on Physics at TeV colliders, dedicated to Thomas Binoth*, Les Houches France, 8–26 Jun 2009 [arXiv:1003.1643] [INSPIRE].

[78] R. Costa, R. Guedes, M.O.P. Sampaio and R. Santos, *ScannerS project* (2014), http://scanners.hepforge.org.

[79] J. Horejsi and M. Kladiva, *Tree-unitarity bounds for THDM Higgs masses revisited*, *Eur. Phys. J.* **C 46** (2006) 81 [hep-ph/0510154] [INSPIRE].

[80] K.G. Klimenko, *Conditions for certain Higgs potentials to be bounded below*, *Theor. Math. Phys.* **62** (1985) 58 [*Teor. Mat. Fiz.* **62** (1985) 87] [INSPIRE].

[81] S.R. Coleman, *Fate of the false vacuum: semiclassical theory*, *Phys. Rev.* **D 15** (1977) 2929 [*Erratum ibid.* **D 16** (1977) 1248] [INSPIRE].

[82] C.G. Callan Jr. and S.R. Coleman, *Fate of the false vacuum. II. First quantum corrections*, *Phys. Rev.* **D 16** (1977) 1762 [INSPIRE].

[83] P.M. Ferreira, R. Santos and A. Barroso, *Stability of the tree-level vacuum in two Higgs doublet models against charge or CP spontaneous violation*, *Phys. Lett.* **B 603** (2004) 219 [*Erratum ibid.* **B 629** (2005) 114] [hep-ph/0406231] [INSPIRE].

[84] H.E. Haber and H.E. Logan, *Radiative corrections to the $Zb\bar{b}$ vertex and constraints on extended Higgs sectors*, *Phys. Rev.* **D 62** (2000) 015011 [hep-ph/9909335] [INSPIRE].

[85] O. Deschamps et al., *The two Higgs doublet of type II facing flavour physics data*, *Phys. Rev.* **D 82** (2010) 073012 [arXiv:0907.5135] [INSPIRE].

[86] F. Mahmoudi and O. Stål, *Flavor constraints on two-Higgs-doublet models with general diagonal Yukawa couplings*, *Phys. Rev.* **D 81** (2010) 035016 [arXiv:0907.1791] [INSPIRE].

JHEP03(2017)094

[87] T. Hermann, M. Misiak and M. Steinhauser, *$\bar{B} \to X_s\gamma$ in the two Higgs doublet model up to next-to-next-to-leading order in QCD*, *JHEP* **11** (2012) 036 [arXiv:1208.2788] [INSPIRE].

[88] M. Misiak et al., *Updated NNLO QCD predictions for the weak radiative B-meson decays*, *Phys. Rev. Lett.* **114** (2015) 221801 [arXiv:1503.01789] [INSPIRE].

[89] W. Grimus, L. Lavoura, O.M. Ogreid and P. Osland, *A precision constraint on multi-Higgs-doublet models*, *J. Phys.* **G 35** (2008) 075001 [arXiv:0711.4022] [INSPIRE].

[90] W. Grimus, L. Lavoura, O.M. Ogreid and P. Osland, *The oblique parameters in multi-Higgs-doublet models*, *Nucl. Phys.* **B 801** (2008) 81 [arXiv:0802.4353] [INSPIRE].

[91] Gfitter Group, M. Baak et al., *The global electroweak fit at NNLO and prospects for the LHC and ILC*, *Eur. Phys. J.* **C 74** (2014) 3046 [arXiv:1407.3792] [INSPIRE].

[92] P. Bechtle, O. Brein, S. Heinemeyer, G. Weiglein and K.E. Williams, *HiggsBounds: confronting arbitrary Higgs sectors with exclusion bounds from LEP and the Tevatron*, *Comput. Phys. Commun.* **181** (2010) 138 [arXiv:0811.4169] [INSPIRE].

[93] P. Bechtle, O. Brein, S. Heinemeyer, G. Weiglein and K.E. Williams, *HiggsBounds 2.0.0: confronting neutral and charged Higgs sector predictions with exclusion bounds from LEP and the Tevatron*, *Comput. Phys. Commun.* **182** (2011) 2605 [arXiv:1102.1898] [INSPIRE].

[94] P. Bechtle et al., *HiggsBounds-4: improved tests of extended Higgs sectors against exclusion bounds from LEP, the Tevatron and the LHC*, *Eur. Phys. J.* **C 74** (2014) 2693 [arXiv:1311.0055] [INSPIRE].

[95] R.V. Harlander, S. Liebler and H. Mantler, *SusHi: a program for the calculation of Higgs production in gluon fusion and bottom-quark annihilation in the standard model and the MSSM*, *Comput. Phys. Commun.* **184** (2013) 1605 [arXiv:1212.3249] [INSPIRE].

[96] R.V. Harlander, S. Liebler and H. Mantler, *SusHi Bento: beyond NNLO and the heavy-top limit*, *Comput. Phys. Commun.* **212** (2017) 239 [arXiv:1605.03190] [INSPIRE].

[97] ATLAS and CMS collaborations, *Measurements of the Higgs boson production and decay rates and constraints on its couplings from a combined ATLAS and CMS analysis of the LHC pp collision data at $\sqrt{s} = 7$ and 8 TeV*, *JHEP* **08** (2016) 045 [arXiv:1606.02266] [INSPIRE].

[98] P.M. Ferreira, J.F. Gunion, H.E. Haber and R. Santos, *Probing wrong-sign Yukawa couplings at the LHC and a future linear collider*, *Phys. Rev.* **D 89** (2014) 115003 [arXiv:1403.4736] [INSPIRE].

[99] P.M. Ferreira, R. Guedes, M.O.P. Sampaio and R. Santos, *Wrong sign and symmetric limits and non-decoupling in 2HDMs*, *JHEP* **12** (2014) 067 [arXiv:1409.6723] [INSPIRE].

[100] D. Fontes, J.C. Romão and J.P. Silva, *Reappraisal of the wrong-sign $hb\bar{b}$ coupling and the study of $h \to Z\gamma$*, *Phys. Rev.* **D 90** (2014) 015021 [arXiv:1406.6080] [INSPIRE].

[101] M. Krause, M. Mühlleitner, R. Santos and H. Ziesche, *2HDM Higgs-to-Higgs decays at next-to-leading order*, arXiv:1609.04185 [INSPIRE].

[102] A. Barroso, P.M. Ferreira and R. Santos, *Neutral minima in two-Higgs doublet models*, *Phys. Lett.* **B 652** (2007) 181 [hep-ph/0702098] [INSPIRE].

[103] I.P. Ivanov, *Minkowski space structure of the Higgs potential in the two-Higgs-doublet model. II. Minima, symmetries and topology*, *Phys. Rev.* **D 77** (2008) 015017 [arXiv:0710.3490] [INSPIRE].

JHEP03(2017)094